AGU PUBLICATIONS

Water Resources Research

RESEARCH ARTICLE
10.1002/2015WR017115

Under-canopy turbulence and root water uptake of a Tibetan meadow ecosystem modeled by Noah-MP

Donghai Zheng[1,2], Rogier Van der Velde[1], Zhongbo Su[1], Jun Wen[3], Martijn J. Booij[2], Arjen Y. Hoekstra[2], and Xin Wang[3]

[1]Faculty of Geo-Information Science and Earth Observation, University of Twente, Enschede, Netherlands, [2]Faculty of Engineering Technology, University of Twente, Enschede, Netherlands, [3]Key laboratory of Land Surface Process and Climate Change in Cold and Arid Regions, Cold and Arid Regions Environmental and Engineering Research Institute, Chinese Academy of Sciences, Lanzhou, China

Key Points:
- Under-canopy turbulence and root water uptake schemes implemented in Noah-MP are augmented
- Impact of the augmentations on Noah-MP performance is evaluated for a Tibetan meadow site
- Simulations of water and heat fluxes by Noah-MP are improved greatly with the augmentations

Correspondence to:
D. Zheng,
d.zheng@utwente.nl

Citation:
Zheng, D., R. van der Velde, Z. Su, J. Wen, M. J. Booij, A. Y. Hoekstra, and X. Wang (2015), Under-canopy turbulence and root water uptake of a Tibetan meadow ecosystem modeled by Noah-MP, *Water Resour. Res.*, *51*, 5735–5755, doi:10.1002/2015WR017115.

Received 19 FEB 2015
Accepted 30 JUN 2015
Accepted article online 3 JUL 2015
Published online 27 JUL 2015

Abstract The Noah-MP land surface model adopts a multiparameterization framework to accommodate various alternative parameterizations for more than 10 physical processes. In this paper, the parameterizations implemented in Noah-MP associated with under-canopy turbulence and root water uptake are enhanced with: (i) an under-canopy turbulence scheme currently adopted by the Community Land Model (CLM), (ii) two vertical root distribution functions, i.e., an exponential and an asymptotic formulation, and (iii) three soil water stress functions (β_t) controlling root water uptake, e.g., a soil water potential (ψ)-based function, a nonlinear soil moisture (θ)-based power function and an empirical threshold approach considering preferential uptake from the moist part of the soil column. A comprehensive data set of in situ micrometeorological observations and profile soil moisture/temperature measurements collected from an alpine meadow site in the northeastern Tibetan Plateau is utilized to assess the impact of the augmentations on the Noah-MP performance. The results indicate that (i) implementation of the CLM under-canopy turbulence scheme greatly resolves the overestimation of sensible heat flux and underestimation of soil temperature across the profile, (ii) both exponential and asymptotic vertical root distribution functions better represent the Tibetan conditions enabling a better representation of the measured soil moisture dynamics, and (iii) the ψ-based β_t functions overestimate surface soil moisture, the default linear θ-based β_t function underestimates latent heat flux during the dry-down, while both the nonlinear power function and empirical threshold approach simultaneously simulate well soil moisture, and latent and sensible heat fluxes. Additionally, the parameter uncertainty associated with soil water stress function and hydraulic parameterization is addressed.

1. Introduction

Land surface models (LSMs) are often employed in atmospheric general circulation models (AGCMs) to provide the lower boundary conditions in the form of moisture and energy exchanges at the land-atmosphere interface, and climatic studies have demonstrated that an accurate quantification of these exchanges is crucial for reliable weather forecast across various time scales [*Koster et al.*, 2004; *Seneviratne et al.*, 2006]. To better represent the complex interplay of the water, energy and nutrient cycles, many of the physical and physiological processes occurring in atmosphere-snow-vegetation-soil-aquifer system have been incorporated into LSM structures [*Clark et al.*, 2015c; *Ek et al.*, 2003; *Luo et al.*, 2013; *Maxwell and Miller*, 2005; *Niu et al.*, 2011; *Oleson et al.*, 2013; *Sellers et al.*, 1986]. However, large discrepancies exist between the model outputs generated by various LSMs even when driven with the same meteorological forcing [*Dirmeyer et al.*, 2006; *Jiménez et al.*, 2011; *Xia et al.*, 2014].

Typical ways of improving LSM performance is to replace the existing parameterization of individual physical or physiological processes with more advanced ones [*Maxwell and Miller*, 2005; *Niu et al.*, 2014], and/or to incorporate missing processes [*Luo et al.*, 2013; *Zeng et al.*, 2011]. However, many parameterizations exist for a particular individual process, and the appropriateness of a parameterization may depend on the type of ecosystem [*Li et al.*, 2011; *Niu et al.*, 2011]. For instance, various vertical root distribution functions [*Chen et al.*, 1996; *Vrugt et al.*, 2001; *Zeng*, 2001] are employed by LSMs to simulate the root water uptake, and the extraction of soil water for transpiration from specific layers [*Feddes et al.*, 1978]. Diversity is also found

among the parameterizations used to compute the soil water availability and severity of soil water stress [*Lai and Katul*, 2000; *Li et al*., 2001; *Verhoef and Egea*, 2014], which introduces large uncertainties as well [*Li et al*., 2013; *Niu et al*., 2011]. In many cases, no clear reason exists for preferring one parameterization over the other [*Gayler et al*., 2014], and the selection of a parameterization in the LSMs is often based on its numerical efficiency [*de Rosnay et al*., 2000; *Ek et al*., 2003]. As such, uncertainties related to the parameterization of specific processes can be of major influence for the model performance [*Ajami et al*., 2007; *Clark et al*., 2008], and an ensemble representation (e.g., multimodel or multiphysics options) can serve in understanding observed processes [*Clark et al*., 2015a; *Dirmeyer et al*., 2006; *Pitman et al*., 2003; *Xia et al*., 2014].

The Noah-MP model [*Niu et al*., 2011] is such an effort initiated to do justice to physical reality by providing multiple parameterization options for various processes within the framework of the community Noah LSM [*Ek et al*., 2003], offering the opportunity to perform ensemble simulations with a single model structure [*Yang et al*., 2011]. Although alternative parameterizations for more than 10 processes (e.g., canopy radiation transfer, vegetation dynamic, stomatal resistance, runoff and groundwater) are implemented, some processes have received little attention. For instance, only a uniform vertical root distribution function is currently available, while parsimonious alternatives exist [*Jackson et al*., 1996; *Li et al*., 2006; *Zeng*, 2001]. Further, a great diversity is also found in the way the effect of soil water stress on plant transpiration and the feedback of root uptake on water availability are defined [*Li et al*., 2013; *Zheng and Wang*, 2007]. Moreover, *Clark et al*. [2015b] recently reported on the uncertainty with the simulated surface energy and water budgets caused by under-canopy turbulence parameterization, while no alternatives have been taken up in the current Noah-MP model. Hence, further augmentation of the Noah-MP LSM and validation against observations remain imperative.

Understanding the land surface processes on the Tibetan Plateau is of great importance for study of the Asian monsoon and management of the Asian water towers [*Immerzeel et al*., 2010; *Yang et al*., 2014; *Zhou et al*., 2009]. Since the 1990s, intensive field campaigns and comprehensive hydro-meteorological observational networks have been and are being developed on the Tibetan Plateau [*Koike*, 2004; *Koike et al*., 1999; *Ma et al*., 2008; *Su et al*., 2011; *Yang et al*., 2013]. The resulting data sets have advanced and will further advance our understanding of the prevailing processes linked to water, energy and nutrient cycles [*Ma et al*., 2009; *Piao et al*., 2012], accompanied with a considerable improvement in the performance of LSMs in the world's highest alpine meadow ecosystem [*Chen et al*., 2011; *van der Velde et al*., 2009; *K. Yang et al*., 2009; *Zheng et al*., 2014]. Imperfection in the ability of state-of-the-art LSMs to reproduce measured soil moisture and soil temperature profiles across the Tibetan Plateau, however, still remains [*Y. Chen et al*., 2013; *Su et al*., 2013; *Xue et al*., 2013]. A major reason for the poor performance of LSMs in this region is the absence of vertical soil heterogeneity within model structures caused by the existence of dense vegetation roots and abundance of organic matter in the topsoil [*Y. Chen et al*., 2013; *Yang et al*., 2005]. Further investigation and improvement of LSMs' performance on the Tibetan Plateau are thus still needed.

In this paper, we seek to further enhance the multiparameterization framework of Noah-MP in representing under-canopy turbulence and root water uptake, as well as to investigate its ability to reproduce simultaneously the surface heat flux and soil moisture/temperature profiles measured in an alpine meadow ecosystem in the northeastern part of the Tibetan Plateau. Noah-MP simulates above-canopy and under-canopy (e.g., within-canopy and below-canopy) turbulence using a two-source model [*Niu et al*., 2011], within which an exponential function parameterizes both the within-canopy and below-canopy turbulent transfers [*Niu and Yang*, 2004]. More recently, *Clark et al*. [2015b] and *Mahat et al*. [2013] suggest the usage of a logarithmic profile for the below canopy and an exponential profile for within-canopy turbulence whereby the bottom of the canopy is the prescribed transition height. Both methods attain the same behavior when the bottom of the canopy layer and the surface roughness length are of the same height as is typically the case for alpine meadow ecosystems. A well-known issue with this approach toward under-canopy turbulence is that the solution does not converge to the bare soil situation once the canopy is removed [*Zeng et al*., 2005]. Moreover, the sensitive parameter (e.g., canopy absorption coefficient) is difficult to specify reliably at global scale [*Sakaguchi and Zeng*, 2009] and its worldwide applicability has been questioned.

Recognizing the inherent complexity in the parameterization of the under-canopy turbulence and the suitability of the exponential decay function for leaf part of vegetation canopies, *Zeng et al*. [2005] proposed an approach that weighs the under-canopy turbulence of a thick canopy and bare soil as function of the area covered by the foliage and stems. Although the weighing based on leaf and stems area coverage is

empirical in nature, the adopted formulations for the under-canopy turbulence transfer, being either thick canopy or bare soil, remain unchanged and physically based. Hence, the approach could also be seen as a way of accounting for the within pixel variability and is yet found to have a similar performance as the more physically based alternatives [*Zeng et al*., 2005]. As a result, the under-canopy turbulence scheme by *Zeng et al*. [2005] is implemented in the Community Land Model (CLM) [*Oleson et al*., 2013], but further evaluation is needed to confirm its validity across a range of ecosystems.

Root water uptake is a sink term to the soil water budget that depends on the root distribution across the soil profile as well as soil water availability. Although a fixed rooting depth adopted in Noah-MP is generally applicable to perennial grasslands, the assumption of a uniform vertical distribution of the roots is invalid for the Tibetan ecosystem that is characterized by an abundance of roots in the topsoil [*Y. Yang et al*., 2009]. *Y. Yang et al*. [2009] and *Zeng* [2001] have developed respectively an asymptotic and an exponential vertical root distribution function to better represent this reality, which are neither available in Noah-MP at present.

Noah-MP does facilitate three options for calculating the soil water availability (f_{sw}) and the soil water stress factor (β_t), namely a linear soil moisture (θ)-based, a linear soil water potential (ψ)-based and an exponential ψ-based function [*Niu et al*., 2011]. However, other alternatives exist that were proven to perform better [*Lawrence and Chase*, 2009; *Li et al*., 2013; *Verhoef and Egea*, 2014]. For instance, *Lawrence and Chase* [2009] found that the linear ψ-based f_{sw} function available in Noah-MP underestimates the transpiration simulated by an earlier version of CLM (i.e., CLM3) [*Oleson et al*., 2004], whereas the f_{sw} function updated for current CLM (i.e., CLM4.5) [*Oleson et al*., 2013] is not included. Further, a θ-based power function is generally preferred to mimic the nonlinear response of root water uptake to soil water stress [*Rodriguez-Iturbe et al*., 1999; *van der Tol et al*., 2008; *Verhoef and Egea*, 2014]. Moreover, root water uptake is a dynamic process that is maximized through mechanisms as preferential root water uptake [*Kuhlmann et al*., 2012; *Zheng and Wang*, 2007], hydraulic redistribution [*Li et al*., 2012; *Scott et al*., 2008] and water-tracking dynamic root growth [*Schymanski et al*., 2009; *Sivandran and Bras*, 2013], which are all processes that are not present within the current Noah-MP model structure.

We present in this paper the augmentation of the Noah-MP with additional options for representing the under-canopy turbulence and root water uptake processes by including (i) the empirical under-canopy turbulence scheme by *Zeng et al*. [2005], (ii) the asymptotic [*Y. Yang et al*., 2009] and the exponential [*Zeng*, 2001] vertical root distribution functions, and (iii) the linear ψ-based f_{sw} function adopted by the current CLM model [*Oleson et al*., 2013], the θ-based power f_{sw} function [*Rodriguez-Iturbe et al*., 1999], and an empirical threshold preferential root water uptake approach [*Jarvis*, 1989; *Zheng and Wang*, 2007]. A comprehensive data set collected at the Maqu station (33.88°N, 102.15°E at an altitude of about 3430 m) from 8 June 2010 to 30 September 2010 is utilized to assess the impact of the augmentations on the Noah-MP performance. The data set includes in situ micrometeorological observations of radiation, precipitation, wind, air temperature and humidity, eddy-covariance (EC) measurements of sensible and latent heat fluxes, and soil moisture/temperature profile measurements as well as soil properties measured in the laboratory (see section 2). The relevant Noah-MP model physics is described in section 3 and the newly added under-canopy turbulence and root water uptake options are presented in section 4. Subsequently, the Noah-MP performance with each of the augmentations is assessed using the Maqu measurements (see section 5), and the sensitivity of the model results to the empirical soil water stress parameters as well as measured uncertainty associated with soil hydraulic parameters are also investigated (see section 6).

2. Observations and Experiments

2.1. Maqu Observation Station

Maqu Climatic and Environmental Observation station (Figure 1) is located in the source region of the Yellow River (SRYR) in the northeastern part of the Tibetan Plateau, with elevations varying from 3200 to 4200 m above sea level (a.s.l.). The landscape in this region is dominated by alpine meadows (e.g., *Cyperaceae* and *Gramineae*) with a height of 15 cm during summers and about 5 cm during winters. The climate is characterized by cold dry winters and rainy summers, with an annual mean air temperature of 1.2°C, and the mean air temperatures of the coldest month (January) and warmest month (July) are −10°C and 11.7°C, respectively. The precipitation is around 500–600 mm annually, with more than 70% falling during the

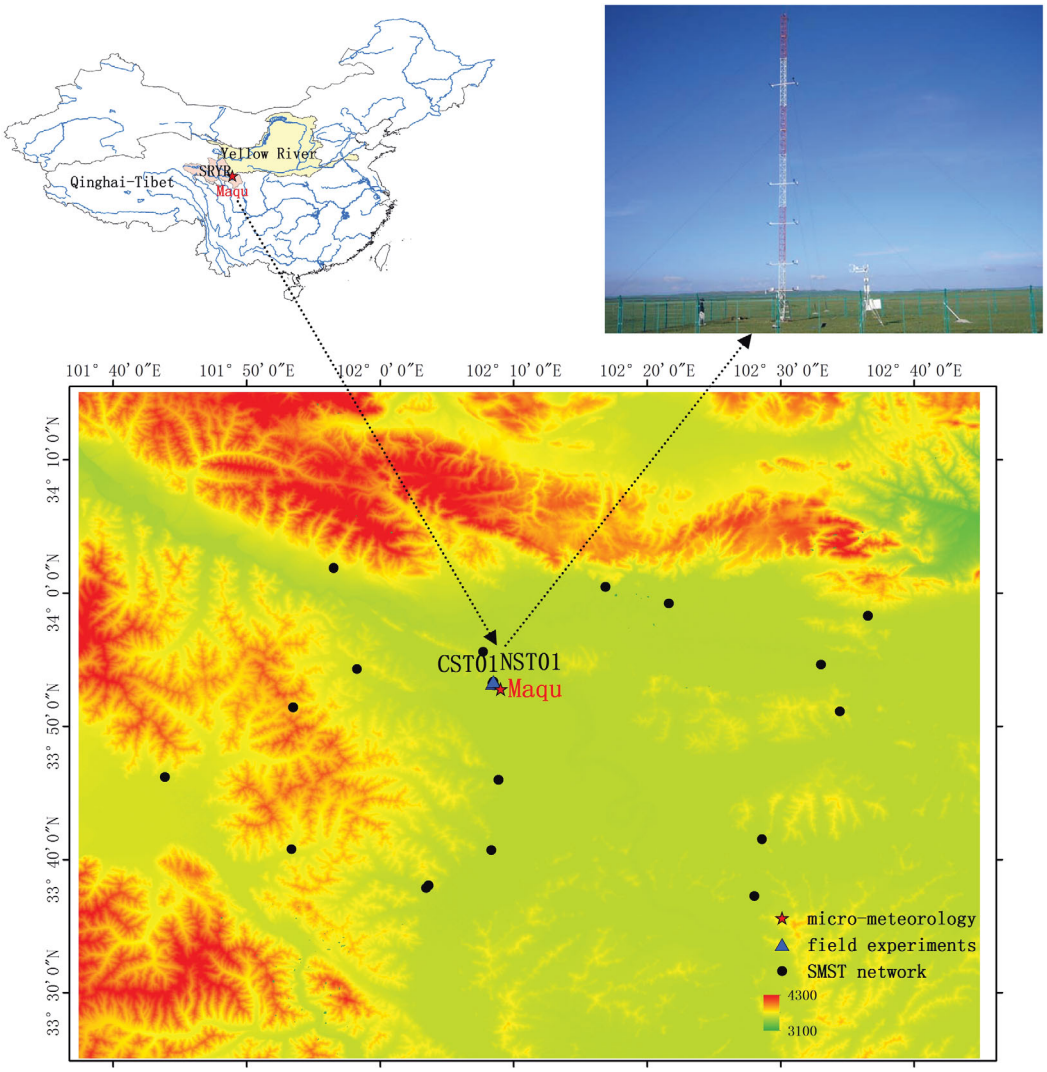

Figure 1. Location of (top left) the source region of the Yellow River (SRYR) in China, (top right) the micrometeorological station and (bottom) the distribution of soil moisture and temperature monitoring stations in the Maqu area shown on top of the 90 m resolution SRTM Digital Elevation Model (DEM).

monsoon season (i.e., between June and September). The groundwater level measured at the station is situated around 8.5–10.0 m below the surface.

The micrometeorological observing system (Figure 1) at the Maqu station consists of a 20 m Planetary Boundary Layer (PBL) tower providing wind speed and direction, air humidity and temperature measurements at five levels (i.e., 18.15, 10.13, 7.17, 4.2, and 2.35 m), and an eddy-covariance (EC) system installed at a height of 3.2 m for measuring the turbulent sensible and latent heat fluxes. Instrumentation for measuring the four radiation components (i.e., upward and downward shortwave and longwave radiations), air pressure and precipitation is also mounted on the PBL tower. A network of 20 soil moisture and soil temperature (SMST) monitoring sites covering an area of 40 km by 80 km centered on the Maqu station is operational since 2008 primarily for the calibration/validation of satellite based soil moisture products [*Dente et al.*, 2012; *Su et al.*, 2011]. Two SMST sites (CST01 and NST01, see Figure 1) of this regional scale network are situated in the vicinity of the micrometeorological station, providing simultaneous soil moisture and temperature measurements for depths of 5, 10, 20, 40 and 80 cm below the soil surface, which are used for the analyses.

The presented investigation spans the period from 8 June 2010 to 30 September 2010. This episode is selected due to the availability of continuous micrometeorological measurements as well as to avoid the

Table 1. Average Values of Soil Hydraulic Parameters Derived From Measurements Performed in the Field and Laboratory[a]

Depth (cm)	Texture	θ_s ($m^3\ m^{-3}$)	K_s ($10^{-6}\ m\ s^{-1}$)	ψ_s (m)	b
5–15	Silt Loam	0.55 (± 0.039)	1.19 (± 0.43)	0.534	7.35
20–40	Silt Loam	0.46 (± 0.042)	0.32 (± 0.17)	0.654	6.40
55–70	Sandy Loam	0.42 (± 0.010)	0.18 (± 0.18)	0.131	3.92

[a]The measured θ_s and K_s ranges are shown in parentheses.

impact of the cold season (e.g., snowpack and frozen soil) processes on the assessment of Noah-MP's soil water flow and heat transport model physics. All the data collected by the micrometeorological observing system and the two SMST sites during this period are reprocessed to values with a 30 min interval. More details on the measurements and data-processing can be found in *Dente et al*. [2012] and *Zheng et al*. [2014].

2.2. Field and Laboratory Experiments

Soil samples were collected around the two SMST sites (CST01 and NST01) to quantify the soil hydraulic properties via laboratory analyses. Three soil profiles were obtained from each site, whereby samples were taken at depths of 10, 30, and 60 cm. Duplicates of undisturbed soil samples were collected by soil cutting ring augers, and field measurements of the saturated hydraulic conductivity (K_s) were carried out with the Guelph Permeameter manufactured by Soilmoisture Equipment Corp.

The soil samples were transported to the laboratory for precise measurement of the soil texture (sand, clay and silt), porosity (θ_s) and soil water retention curve. The soil texture was measured with a Malvern Mastersizer 2000 particle size analyzer, and the soil porosity is calculated from the difference of the saturated and dry soil weight of the cutting ring with known volume (100 cm^3). Soil water contents for 11 pressure heads from 0 up to 15 bar were determined with the Pressure Membrane Instrument manufactured by Soilmoisture Equipment Corp.

The empirical soil hydraulic scheme proposed by *Campbell* [1974] is utilized within the Noah-MP LSM to parameterize the ψ-θ and K-θ relationships as a function of soil texture:

$$\psi(\theta)=\psi_s(\theta/\theta_s)^{-b} \tag{1a}$$

$$K(\theta)=K_s(\theta/\theta_s)^{2b+3} \tag{1b}$$

where ψ_s is the soil water potential at air-entry (m), K_s is the saturated hydraulic conductivity ($m\ s^{-1}$), θ_s is the porosity ($m^3\ m^{-3}$), and b is an empirical parameter related to the pore-size distribution of the soil matrix. The parameters θ_s and K_s are measured directly, while the parameters ψ_s and b are derived via fitting all the measured soil water retention data with equation (1a). The fitted ψ_s and b as well as mean and measured θ_s and K_s range are listed in Table 1.

3. Noah-MP Land Surface Model

The Noah-MP LSM [*Niu et al*., 2011] is an augmented version of the community Noah LSM [*Ek et al*., 2003] designed to form the land component of the research and operational weather forecasting systems of the National Centers for Environment Prediction (NCEP). The improved physics includes differentiation between the role of the vegetation and the soil surface within surface energy balance computations [*Niu and Yang*, 2004], a multilayer snow scheme [*Yang and Niu*, 2003], a simple groundwater module [*Niu et al*., 2007], and a short-term dynamic vegetation scheme as representation of the carbon budget [*Dickinson et al*., 1998]. Noah-MP adopts the same four layer soil scheme as Noah with the thermal diffusion equation for simulating heat transport and the diffusivity form of Richards's equation for water flow [*Mahrt and Pan*, 1984; *Pan and Mahrt*, 1987]. In addition to Noah's original runoff production scheme that accounts only for infiltration-excess surface runoff and free drainage base flow [*Schaake et al*., 1996], Noah-MP also includes saturation-excess surface runoff and groundwater impact on base flow following the simple TOPMODEL-based runoff parameterization [*Niu et al*., 2005].

Noah-MP also accommodates a multiparameterization framework [*Niu et al*., 2011] for canopy radiation transfer, dynamic vegetation, stomatal resistance, soil water stress, aerodynamic resistance, runoff and

groundwater. More than one parameterization is included for 10 physical processes making up for a total of 4608 combinations [*Gayler et al.*, 2014]. The Noah-MP model physics associated with the surface energy balance and under-canopy turbulence, soil water flow and root water uptake are given below. Additional information on, for instance, the runoff production and groundwater generation can be found in *Niu et al.* [2011].

3.1. Surface Energy Balance and Under-Canopy Turbulence

Noah-MP adopts a "semitile" approach to enable differentiation of the surface energy balance processes from vegetation, vegetation covered ground and bare ground within a single grid cell as follows:

$$S_v = F_{veg}[L_v(T_v) + LE_v(T_v) + H_v(T_v)] \tag{2a}$$

$$F_{veg}S_g = F_{veg}[L_{g,v}(T_{g,v}) + LE_{g,v}(T_{g,v}) + H_{g,v}(T_{g,v}) + G_{g,v}(T_{g,v})] \tag{2b}$$

$$(1-F_{veg})S_g = (1-F_{veg})[L_{g,b}(T_{g,b}) + LE_{g,b}(T_{g,b}) + H_{g,b}(T_{g,b}) + G_{g,b}(T_{g,b})] \tag{2c}$$

where F_{veg} is the green vegetation fraction, S_v is the net shortwave radiation absorbed by the vegetation canopy (W m^{-2}), S_g is the net shortwave radiation absorbed by vegetation covered ground and bare ground (W m^{-2}), L is the net longwave radiation (W m^{-2}), LE is the latent heat flux (W m^{-2}), H is the sensible heat flux (W m^{-2}), G is the ground heat flux (W m^{-2}), T is the temperature (K), and the subscripts "v", "g,v", and "g,b" refer to vegetation canopy, ground surface under vegetation canopy, and bare soil ground surface.

The semitile scheme computes S over the entire grid using a modified two-stream approximation with consideration of partial vegetation coverage [*Niu and Yang*, 2004]. The two-stream radiation scheme accounts for scattering and multiple reflections by the canopy and ground in two mainstreams of radiative fluxes (i.e., vertical upward and downward) for the visible and near-infrared part of the spectrum. Other surface energy budget components (e.g., L, LE, H, and G) are computed as sum of the fluxes produced by the vegetation fraction (F_{veg}) and bare ground fraction ($1 - F_{veg}$). Vegetation canopy (T_v), vegetation covered ground ($T_{g,v}$) and bare ground skin temperature ($T_{g,b}$) are solved iteratively through equations (2a)–(2c) using the Newton-Raphson method.

In Noah-MP, the under-canopy turbulence (i.e., $LE_{g,v}$ and $H_{g,v}$ in equation (2b)) is computed as:

$$H_{g,v} = \rho c_p \frac{T_{g,v} - T_{ac}}{r_{a,g}} \tag{3a}$$

$$LE_{g,v} = \rho \frac{rh_{eq} \cdot q_{sat}(T_{g,v}) - q_{ac}}{r_{a,g} + r_{soil}} \tag{3b}$$

where ρ is the air density (kg m^{-3}), c_p is the specific heat of air (J kg^{-1} K^{-1}), T_{ac} and q_{ac} are respectively the air temperature (K) and the specific humidity (kg kg^{-1}) within the canopy, $q_{sat}(T_{g,v})$ is the saturated specific humidity at the ground temperature (kg kg^{-1}), rh_{eq} is the equilibrium relative humidity of air within the soil matrix, r_{soil} is the soil surface resistance (s m^{-1}), and $r_{a,g}$ is the aerodynamic resistance below the canopy (s m^{-1}) formulated as [*Niu and Yang*, 2004]:

$$r_{a,g} = \frac{h_c}{a \cdot \kappa u_*(h_c - d_0)} \left\{ \exp\left[a(1 - z_{0g}/h_c)\right] - \exp\left[a(1 - (z_{0v} + d_0)/h_c)\right] \right\} \tag{4a}$$

$$a = [c_d \cdot h_c \cdot (LAI + SAI)/l_m]^{0.5} (\Phi_m)^{0.5} \tag{4b}$$

where h_c is the canopy height (m), z_{0g} is ground roughness length taken as 0.01 m, z_{0v} is the canopy roughness length taken as $0.12h_c$ (m), d_0 is the zero displacement height taken as $0.65h_c$ (m), κ is the von Karman constant taken as 0.4, u^* is the friction velocity (m s^{-1}), a is the absorption coefficient of momentum, c_d is the drag coefficient of leaves, LAI is the leaf area index (m^2 m^{-2}), SAI is the stem area index (m^2 m^{-2}), l_m is the mean mixing length (m), and Φ_m is the stability correction factor for momentum transfer. The values of c_d and l_m are prescribed in Noah-MP as 0.2 and 1.13 m for global applications even though this parameterization is strictly speaking developed for coniferous trees [*Niu and Yang*, 2004] as will be further elaborated on in section 4.1.

3.2. Soil Water Flow and Root Water Uptake

The diffusivity form of Richards's equation is adopted by Noah-MP for the simulation of soil water flow:

$$\frac{\partial\theta}{\partial t}=\frac{\partial}{\partial z}\left(D(\theta)\frac{\partial\theta}{\partial z}\right)+\frac{\partial K(\theta)}{\partial z}+S_S(\theta) \tag{5}$$

where θ is the soil moisture content ($m^3\ m^{-3}$), t is the time (s), D is the soil water diffusivity ($m^2\ s^{-1}$), K is the hydraulic conductivity ($m\ s^{-1}$), z is the soil depth (m), S_S represents sources and sinks (i.e., precipitation and evapotranspiration, $m\ s^{-1}$).

Root water uptake for evapotranspiration is the main sink term (S_S) of equation (5) and is one of the drivers for the redistribution of water in the soil column. The total transpiration (E_t) is allocated to each soil layer according to an effective root fraction ($r_{e,i}$):

$$E_{t,i}=E_t\cdot r_{e,i} \tag{6}$$

Both E_t and $r_{e,i}$ are influenced by the soil water availability whereby in Noah-MP the impact on E_t is implemented by reducing the stomatal conductance via a soil water stress factor, β_t [*Niu et al.*, 2011]. The soil water stress function, β_t, depends on the water availability across the soil profile and the vertical root distribution as,

$$\beta_t=\sum_{i=1}^{nroot} f_{sw,i}\cdot f_{root,i} \tag{7}$$

where *nroot* is the total number of root layers, $f_{sw,i}$ and $f_{root,i}$ are the soil water availability and root fractions of the i^{th} soil layer.

The effective root fraction, $r_{e,i}$, of the i^{th} soil layer is formulated as:

$$r_{e,i}=\frac{f_{sw,i}\cdot f_{root,i}}{\beta_t} \tag{8}$$

The vertical root distribution f_{root} is assumed to be vertically uniform as:

$$f_{root,i}=\frac{\Delta z_i}{\sum_{i=1}^{nroot}\Delta z_i} \tag{9}$$

where Δz_i is the depth of the i^{th} soil layer (m).

Noah-MP provides three options for the quantification of the soil water availability (f_{sw}): the soil moisture based (1) Noah type, and the soil water potential based (2) CLM type and (3) SSiB type. The Noah-type f_{sw} factor is parameterized as:

$$f_{sw,i}=\frac{\theta_i-\theta_w}{\theta_c-\theta_w} \tag{10}$$

where θ_i is the soil moisture of the i^{th} soil layer ($m^3\ m^{-3}$), θ_w is the soil moisture content at wilting point ($m^3\ m^{-3}$), θ_c is the critical soil moisture content ($m^3\ m^{-3}$) below which the simulated transpiration is reduced due to water stress. In Noah-MP, θ_c is defined at a drainage flux of 0.5 mm d^{-1} and wilting point θ_w is taken at $\psi=-200$ m.

Noah-MP also facilitates the usage of a f_{sw} function implemented in an earlier version of the CLM model (e.g., CLM3) [*Oleson et al.*, 2004]:

$$f_{sw,i}=\frac{\psi_w-\psi_i}{\psi_w-\psi_s} \tag{11}$$

where ψ_w is the soil water potential at wilting point taken as -150 m, ψ_s is a soil type specific saturated soil water potential (m), and ψ_i is the soil water potential of the i^{th} layer computed using equation (1a).

The SSiB-type f_{sw} function is an empirical equation developed by *Xue et al.* [1991] via numerical experiments for global application:

$$f_{sw,i}=1-\exp\left[-c_2\cdot(c_1-\ln(\psi_i))\right] \tag{12}$$

where c_1 and c_2 are vegetation-type specific parameters, c_1 represents the point at which stomata are fully closed (i.e., $c_1=\ln(\psi_w)$), and c_2 is the slope factor. In Noah-MP, ψ_w and c_2 are taken as -150 m and 5.8 respectively independent of the vegetation type [*Niu et al.*, 2011].

4. Additional Under-Canopy Turbulence and Root Water Uptake Consideration

4.1. Under-Canopy Turbulence

As pointed out by *Niu and Yang* [2004] and *Clark et al*. [2015b], the under-canopy turbulence (e.g., $H_{g,v}$) strongly depends on the canopy absorption coefficient of momentum (a, equation (4b)), which is difficult to specify globally [*Sakaguchi and Zeng*, 2009], and the applicability of the coniferous tree parameterization for other vegetation types is questionable. *Brutsaert* [1982] indicated that the exponential decay as function of depth below the top of the vegetation canopy (e.g., equation (4a)) is generally accepted for the leaf part of dense, uniform, and tall vegetation canopies. On the other hand, *Zeng et al*. [2005] showed that the exponential function does not converge to the bare soil formulation as the canopy disappears.

Recognizing this imperfection in the representation of under-canopy turbulence, *Zeng et al*. [2005] proposed an approach that interpolates between the under-canopy turbulent transfer coefficients (C_s) of a thick canopy and bare soil as a function of the sum of the *LAI* and Stem Area Index, *SAI*:

$$r_{a,g}=(C_s\cdot u_*)^{-1} \tag{13a}$$

$$C_s=0.004\cdot[1-\exp(-(LAI+SAI))]+\frac{\kappa}{\alpha}\left(\frac{z_{0g}\cdot u_*}{\nu}\right)^{-0.45}\cdot\exp(-(LAI+SAI)) \tag{13b}$$

where ν is the kinematic molecular viscosity taken as 1.5×10^{-5} m^2 s^{-1}, and α is a constant taken as 0.36 as suggested by *Zeng et al*. [2012]. Above empirical equations are also adopted by current CLM model [*Oleson et al*., 2013] for the calculation of under-canopy turbulence.

4.2. Vertical Root Distribution

The vertical distribution of vegetation roots determines the overall water uptake (equations (6) and (7)) and the relative rates extracted from individual soil layers for transpiration (equation (8)). Considerably, different root distributions are implemented in the state-of-the-art LSMs [*Zeng*, 2001]. For instance, both Noah and Noah-MP LSMs adopt by default a uniform vertical distribution of roots across the soil profile (equation (9)), whereas CLM [*Oleson et al*., 2013] uses an exponential function proposed by *Zeng* [2001]:

$$Y=1-0.5\cdot(\exp(-r_{ta}\cdot d)+\exp(-r_{tb}\cdot d)) \tag{14}$$

where Y is the cumulative root fraction from the soil surface to depth d (m), and r_{ta} and r_{tb} are plant-dependent root distribution parameters prescribed by *Zeng* [2001] for global applications respectively as 10.74 m^{-1} and 2.608 m^{-1} for grassland.

Another widely used root distribution function is the asymptotic formulation proposed by *Gale and Grigal* [1987]:

$$Y=1-\beta^{d\cdot100} \tag{15}$$

where 100 is the factor to convert the unit of soil depth d from m to cm, β is an empirical fitting parameter that defines the vertical root distribution. *Jackson et al*. [1996] estimated the β parameter from measurements for various natural biomes across the globe. *Y. Yang et al*. [2009] more recently reported for the Tibetan Plateau values of 0.937 for alpine steppe and 0.900 for alpine meadow. The latter is applicable for our study area.

The uniform root distribution (equation (9)) implemented by default in Noah and Noah-MP can be replaced with the exponential function resulting in:

$$f_{root,i}=\begin{cases}\dfrac{1-0.5\cdot[\exp(-r_a\cdot\Delta z_i)+\exp(-r_b\cdot\Delta z_i)]}{1-0.5\cdot[\exp(-r_a\cdot\sum_{i=1}^{nroot}\Delta z_i)+\exp(-r_b\cdot\sum_{i=1}^{nroot}\Delta z_i)]}, & i=1\\ \dfrac{1-0.5\cdot[\exp(-r_a\cdot\sum_{j=1}^{i}\Delta z_j)+\exp(-r_b\cdot\sum_{j=1}^{i}\Delta z_j)]}{1-0.5\cdot[\exp(-r_a\cdot\sum_{i=1}^{nroot}\Delta z_i)+\exp(-r_b\cdot\sum_{i=1}^{nroot}\Delta z_i)]}-f_{root,i-1}, & 1<i\le nroot\end{cases} \tag{16}$$

and by the asymptotic function resulting in:

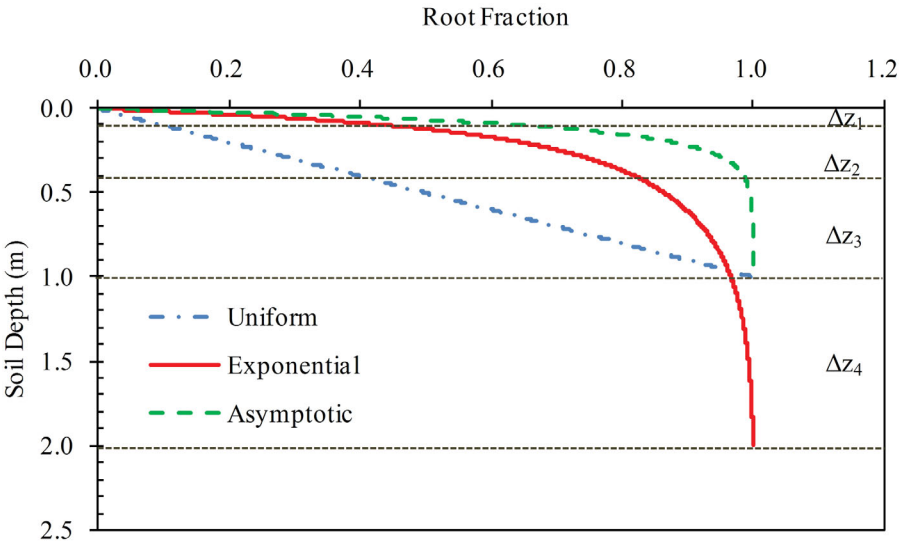

Figure 2. Cumulative root distributions across the 2 m Noah-MP soil column estimated for alpine meadow using (i) a uniform (equation (9)), (ii) an exponential (equation (16)), and (iii) an asymptotic (equation (17)) functions.

$$f_{root,i}=\begin{cases}\dfrac{1-\beta^{\Delta z_i\cdot 100}}{1-\beta^{\sum_{i=1}^{nroot}\Delta z_i\cdot 100}}, i=1\\ \dfrac{1-\beta^{\sum_{j=1}^{i}\Delta z_j\cdot 100}}{1-\beta^{\sum_{i=1}^{nroot}\Delta z_i\cdot 100}}-f_{root,i-1}, 1<i\le nroot\end{cases} \tag{17}$$

where Δz is the depth of each soil layer (m), whereby Noah-MP includes a 2 m soil column with four layers of 0.1, 0.3, 0.6 and 1.0 m. The total rooting depth is defined as the depth at which the cumulative root fraction Y reaches a threshold herein taken as 99% [*Zeng*, 2001]. As such, the total number of root layers (*nroot*) and its vertical distribution are known. Figure 2 shows the estimated vertical root distributions using above three root distribution functions applied for the Tibetan alpine meadow. The figure illustrates that both the exponential (equation (16)) and asymptotic functions (equation (17)) produce a much larger root density in the top 10 cm than the uniform root distribution (equation (9)). This is more in line with reality for the alpine meadows on the Tibetan Plateau [*van der Velde et al*., 2009; *Y. Yang et al*., 2009]. Further, it is noted that the exponential root distribution function provides a deeper rooting depth than the other two functions, e.g., four versus three root layers. Of course, one could question whether vegetation roots are present below 1 m in an alpine meadows ecosystem. It is, however, rather difficult to collect a robust set of in situ measurements that is able to confirm this. We refrain ourselves here from making a quantitative statement on the appropriateness of the root distribution functions and their suitably will be discussed based on the comparison of the measured and simulated soil moisture profiles (see section 5.2).

4.3. Soil Water Stress

Apart from the depth and distribution of roots across the soil profile, the root uptake is also constrained by the water availability (equations (6) and (7)). Whereas the root distribution (f_{root}) can be derived from measurements, it remains difficult to unambiguously describe the response of root uptake to soil water availability (e.g., f_{sw}). Various linear or nonlinear empirical formulations based on either soil moisture (θ) or soil water potential (ψ) are utilized by LSMs [e.g., *Chen et al*., 1996; *Oleson et al*., 2013; *Sellers et al*., 1986]. Noah-MP facilitates three options for the computation of f_{sw} (see equations (10)–(12)) to reflect the great uncertainty involved with its implementation [*Niu et al*., 2011].

Here we also consider the updated version of the CLM3 parameterization (equation (11)) that has been included in latest CLM version 4.5 (CLM4.5) [*Oleson et al*., 2013] as *Lawrence and Chase* [2009] found its predecessor underestimating transpiration globally. In the revised formulation the critical soil water potential is defined based on plant physiological principles and reads,

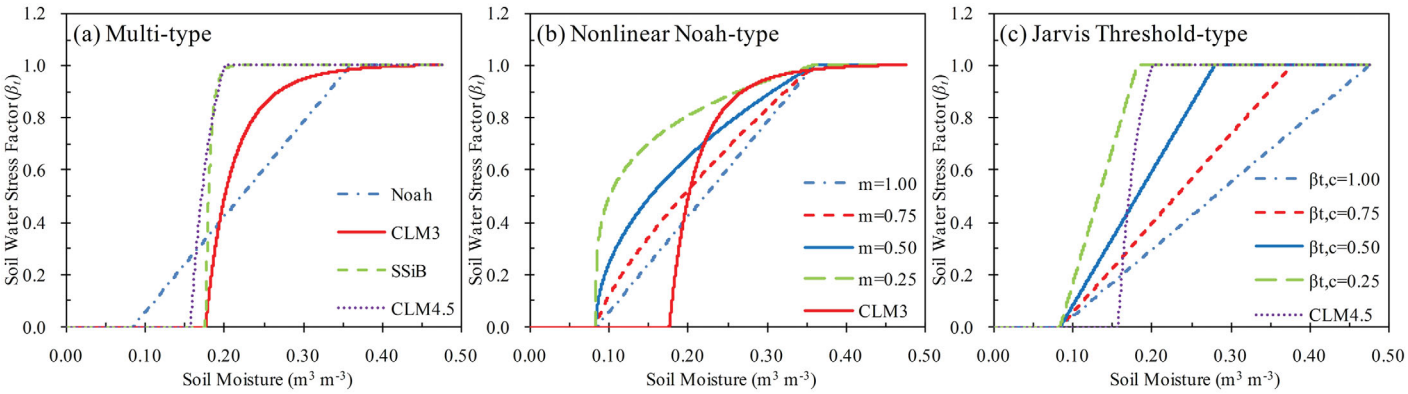

Figure 3. Soil water stress factors (β_t) controlling water uptake of alpine meadow in a silt loam soil as a function of soil moisture computed with (a) four types of parameterizations, (b) a nonlinear soil moisture-based water stress formulation with various values for power *m* (equation (19)), and (c) a Jarvis threshold approach with different threshold values ($\beta_{t,c}$, equations (20a) and (20b)).

$$f_{sw,i} = \frac{\psi_c - \psi_i}{\psi_c - \psi_o} \tag{18}$$

where ψ_c and ψ_o are plant-type specific soil water potentials (m) when stomata are fully closed or fully open prescribed for grassland as -275 m and -74 m, respectively.

Figure 3a shows the estimated soil water stress factor β_t (equation (7)) as a function of soil moisture computed with the four f_{sw} functions for alpine meadow on a silt loam soil type assuming a homogeneous soil texture profile. The CLM4.5 parameterization (equation (18)) behaves almost identical to the SSiB one (equation (12)) whereby the soil water constraint on root uptake starts at low moisture levels (< 0.20 m^3 m^{-3}) and fully shuts down transpiration under still fairly wet conditions (> 0.15 m^3 m^{-3}). The CLM3 f_{sw} function (equation (11)) stands for a more gradual decline of the root uptake that commences already near saturation and completely stops transpiration at similar moisture levels as the SSiB and CLM4 parameterizations. On the other hand, the Noah θ-based parameterization (equation (10)) poses the strongest constraint under wet conditions, but enables the root uptake shutdown under much drier conditions (< 0.10 m^3 m^{-3}) as compared to the other three ψ-based f_{sw} functions.

Based on the findings above, we also adopt a nonlinear θ-based f_{sw} formulation parameterized with a power *m* for mitigating the excessive constraint on the root uptake under wet conditions, while enabling transpiration up to soil moisture contents below 0.10 m^3 m^{-3},

$$f_{sw,i} = \left(\frac{\theta_i - \theta_w}{\theta_c - \theta_w}\right)^m \tag{19}$$

The power, *m*, added to the linear θ-based f_{sw} function is similar to the work of *Rodriguez-Iturbe et al.* [1999], *van der Tol et al.* [2008], and *Verhoef and Egea* [2014] to represent more realistically the nonlinear response of vegetation transpiration and root water uptake to the f_{sw}. The parameter *m* is purely empirical forcing equation (19) to be linear once *m* is equal to 1.0, while lower values produce weaker constraints on the root uptake as shown in Figure 3b.

Further it should be noted that plants have the ability to mitigate the effects of stress by preferentially taking up water from the moist portions of the root zone [*Lai and Katul*, 2000; *Li et al.*, 2001] enabling plants to transpire at its full capacity even though parts of the root system are water limited [*Zheng and Wang*, 2007]. In other words, water stress in a specific soil layer does not necessarily implicate water stress at the plant level, which is at present not accounted for. The approach originally proposed by *Jarvis* [1989] and refined by *Zheng and Wang* [2007] is adopted to allow the plants to maintain full capacity transpiration in presence of water stress in a portion of the soil profile:

$$\beta_t = \begin{cases} 1.0, & \beta_{t,0} \geq \beta_{t,c} \\ \beta_{t,0}/\beta_{t,c}, & \beta_{t,0} < \beta_{t,c} \end{cases} \tag{20a}$$

Table 2. List of Numerical Experiments Designed to Evaluate the Noah-MP Performance With Various Under-Canopy Turbulence, Vertical Vegetation Root Distribution and Soil Water Stress Parameterizations

Processes	Options	Experiments
Under-canopy turbulence (UCT)	UCT=1: original Noah-MP (equations (4a) and (4b))	EXP1a
	=2: *Zeng et al.* [2005] (equations (13a) and (13b))	EXP1b
Vertical root distribution (VRT)	VRT=1: uniform distribution (equation (9))	EXP2a
	=2: exponential function (equation (16))	EXP2b
	=3: asymptotic function (equation (17))	EXP2c
Soil water stress (SWS)	SWS=1: Noah (equations (7) and (10))	EXP3a
	=2: CLM3 (equations (7) and (11))	EXP3b
	=3: SSiB (equations (7) and (12))	EXP3c
	=4: CLM4.5 (equations (7) and (18))	EXP3d
	=5: nonlinear Noah (equations (7) and (19))	EXP3e
	=6: Jarvis threshold (equations (20a) and (20b))	EXP3f

$$\beta_{t,0}=\sum_{i=1}^{nroot} f_{root,i}\cdot\frac{\theta_i-\theta_w}{\theta_s-\theta_w} \tag{20b}$$

where $\beta_{t,c}$ is a tunable threshold value between 0.0 and 1.0. Water stress at the whole plant level is not triggered as long as the local level water stress factor $\beta_{t,0}$ remains above a certain threshold $\beta_{t,c}$. Once $\beta_{t,0}$ drops below the $\beta_{t,c}$, water limited plant transpiration is produced. The performance of the Jarvis's threshold approach is identical to the linear θ-based (e.g., Noah-type) stress function when $\beta_{t,c}$ is taken equal to 1.0 and approaches the CLM4 under wet conditions with low $\beta_{t,c}$ values as shown in Figure 3c.

4.4. Design of Numerical Experiments

Noah-MP provides a flexible way of adding new parameterizations for a variety of physical processes. For this investigation, we employ the offline 1D Noah-MP LSM version 1.1. The Noah-MP code is augmented to include the additional options for under-canopy turbulence (see section 4.1), vertical distribution of roots (see section 4.2), soil water stress function (see section 4.3), and to utilize the measured soil hydraulic functions (see Table 1).

Three groups of numerical experiments are performed to investigate the impact of the (i) under-canopy turbulence, (ii) root distribution, and (iii) soil water stress parameterizations on the surface heat flux and states (e.g., moisture and temperature) simulated across the soil profile. Firstly, the performance of Noah-MP with the default under-canopy turbulence scheme (equations (4a) and (4b), hereafter EXP1a) and the one proposed by *Zeng et al*. [2005] (equations (13a) and (13b), EXP1b) are assessed, whereby the default uniform vertical root distribution (equation (9)) and water stress function (equations (7) and (10)) are invoked. Second, the Noah-MP performance is evaluated with the default uniform (EXP2a), the exponential (equation (16), EXP2b) and the asymptotic (equation (17), EXP2c) root distribution functions, while the default water stress function and the superior under-canopy turbulence scheme following from the first experiment are utilized. Third, the performance of Noah-MP with six different soil water stress functions is investigated (hereafter EXP3a–3f, respectively): (i) default Noah (equation (10)), (ii) CLM3 (equation (11)), (iii) SSiB (equation (12)), (iv) CLM4 (equation (18)), (v) nonlinear Noah (equation (19)), and (vi) Jarvis (equations (20a) and (20b)) using the best performing under-canopy turbulence and vertical root distribution schemes selected based on the previous two experiments. It is noted that the empirical power, *m*, in equation (19) for EXP3e and threshold $\beta_{t,c}$ in equation (20a) for EXP3f are both taken as 0.5. The three groups of numerical experiments are summarized in Table 2. For each experiment, Noah-MP is run with the following additional parameterizations: (i) monthly values of *LAI* and F_{veg} derived from 10 daily synthesis SPOT *NDVI* product as in *Zheng et al*. [2014] and *X. Chen et al*. [2013], (ii) a stomatal resistance scheme of Jarvis [*Chen et al*., 1996; *Niu et al*., 2011], (iii) the default Noah runoff and drainage scheme as described in *Schaake et al*. [1996] and *Niu et al*. [2011], and (iv) other processes, such as radiation transfer and aerodynamic resistance, as recommended by *Yang et al*. [2011] and *Cai et al*. [2014].

All the experiments are forced by the meteorological measurements collected from 8 June 2010 to 30 September 2010 at Maqu station, which include air temperature, relative humidity, wind speed and wind direction, downward shortwave and longwave radiations, air pressure and precipitation (see section 2.1). The observation height of the air temperature and wind speed is 2.35 m. Grassland is the prescribed vegetation type with the heights for canopy top (h_c) and base set at 0.35 m and 0.01 m respectively, and the canopy roughness length (z_{0v}) is taken as 0.035 m as in *Zheng et al*. [2014]. The leaf reflectance in the near-infrared

is taken as 0.50. Silt loam is the soil type according to the texture measurements (see Table 1). The average values of the measured hydraulic parameters available for the three upper soil layers are adopted and the parameterization for the fourth layer is set equal to that of the third layer. The other parameters are obtained from Noah-MP's default look-up table with the exception of *SAI* that is estimated as recommended by *Zeng et al*. [2002].

Soil moisture and temperature measurements are used to initialize each model run and to validate Noah-MP simulations. The measurements collected at sites CST01 and NST01 are for both initialization and validation averaged for each soil depth (i.e., 0.05, 0.10, 0.20, 0.40, and 0.80 m), and subsequently linearly interpolated to the midpoints of the upper three model layers (i.e., 0.05, 0.25 and 0.70 m). The soil moisture and temperature of the fourth layer is taken equal to the states of the third layer for the initialization. The Noah-MP simulations are further validated through comparisons of the simulated latent heat flux (*LE*) and sensible heat flux (*H*) with measurements collected by the eddy-covariance (EC) system at Maqu station.

5. Noah-MP Simulations

5.1. Under-Canopy Turbulence

Figure 4 shows the mean diurnal cycle of the net incoming (R_n) radiation, turbulent heat fluxes (*LE* and *H*), and the 25 cm and 70 cm soil temperatures measured and simulated by Noah-MP for the months June, July, August and September with two under-canopy turbulence transfer schemes (see Table 2). Table 3 provides the corresponding root mean squared error (RMSE) computed between the measurements and simulations. A general analysis of the measurements (blue line, Figure 4) reveals that *LE* is, on average, more than twice as large as *H* during daytime. Noah-MP with both under-canopy turbulence transfer schemes reproduce comparable and reasonably well R_n (Figure 4a), with a RMSE of around 17 W m^{-2}. Moreover, Noah-MP captures regardless of the under-canopy turbulence scheme also the monthly mean diurnal *LE* cycle quite well with exception of the month September for which the daytime *LE* is underestimated by 50 W m^{-2} (Figure 4b).

Noah-MP with the default under-canopy turbulence transfer scheme (EXP1a) significantly overestimates *H* (Figure 4c) and underestimates the deep soil temperature (Figures 4d and 4e). This is greatly resolved when the scheme proposed by *Zeng et al*. [2005] is used (EXP1b). The parameterization by *Zeng et al*. [2005] produces in comparison to the default one a larger aerodynamic resistance within the canopy ($r_{a,g}$) suppressing the under-canopy turbulence (e.g., equation (3a)) and thereby mitigating the *H* overestimation found for EXP1a. This causes a reduction of about 27% in the RMSE. As less energy is used for the production of turbulent heat, more is available for warming the soil column via ground heat flux (see equations (2b) and (2c)) leading to a better match of the measured and simulated soil temperature profile as well. Improvements of 65% and 81% are noted for the RMSEs computed between the measured and simulated 25 cm (T_{s25}) and 70 cm (T_{s70}) soil temperature. Hence, the under-canopy turbulence scheme of *Zeng et al*. [2005] is selected for the two following experiments.

5.2. Vertical Root Distribution

Figure 5 shows time series of the soil moisture profile measurements with a 30 min interval and simulations produced by Noah-MP with the three vertical root distribution functions (see Table 2) along with the measured rainfall. The upper, mid and lower panels provide the soil moisture measurements and simulations for depths of 5 cm (SM_5), 25 cm (SM_{25}), and 70 cm (SM_{70}), respectively. The SM_5 plot illustrates that the study period holds three distinct dry-down episodes (periods in which the soil moisture is gradually depleted), e.g., (i) DOYs (Days of Year) 159–178, (ii) DOYs 204–222, and (iii) DOYs 249–265, each followed by a wet period with a sequence of substantial rain events, e.g., DOYs 179–203, DOYs 223–248 and DOY 266-onward.

Noah-MP with the default uniform vertical root distribution function (EXP2a) overestimates SM_5 during the second and third dry-downs and SM_{25} starting from the second wet period (e.g., DOY 244-onward), while it underestimates SM_{70} starting from the second dry-down period (e.g., DOY 204-onward). These imperfections in the EXP2a simulated soil moisture profiles are associated with the assumed uniform root distribution that imposes a root water uptake proportional to the layer thickness with respect to the total column depth. This is, however, hardly ever the case in reality. The majority of the plant roots are typically situated in the upper part of the soil column, particularly in Tibetan meadow ecosystems [*Y. Yang et al*., 2009]. The exponential as well as the asymptotic root distribution functions better reflect this reality, which allows Noah-MP to extract

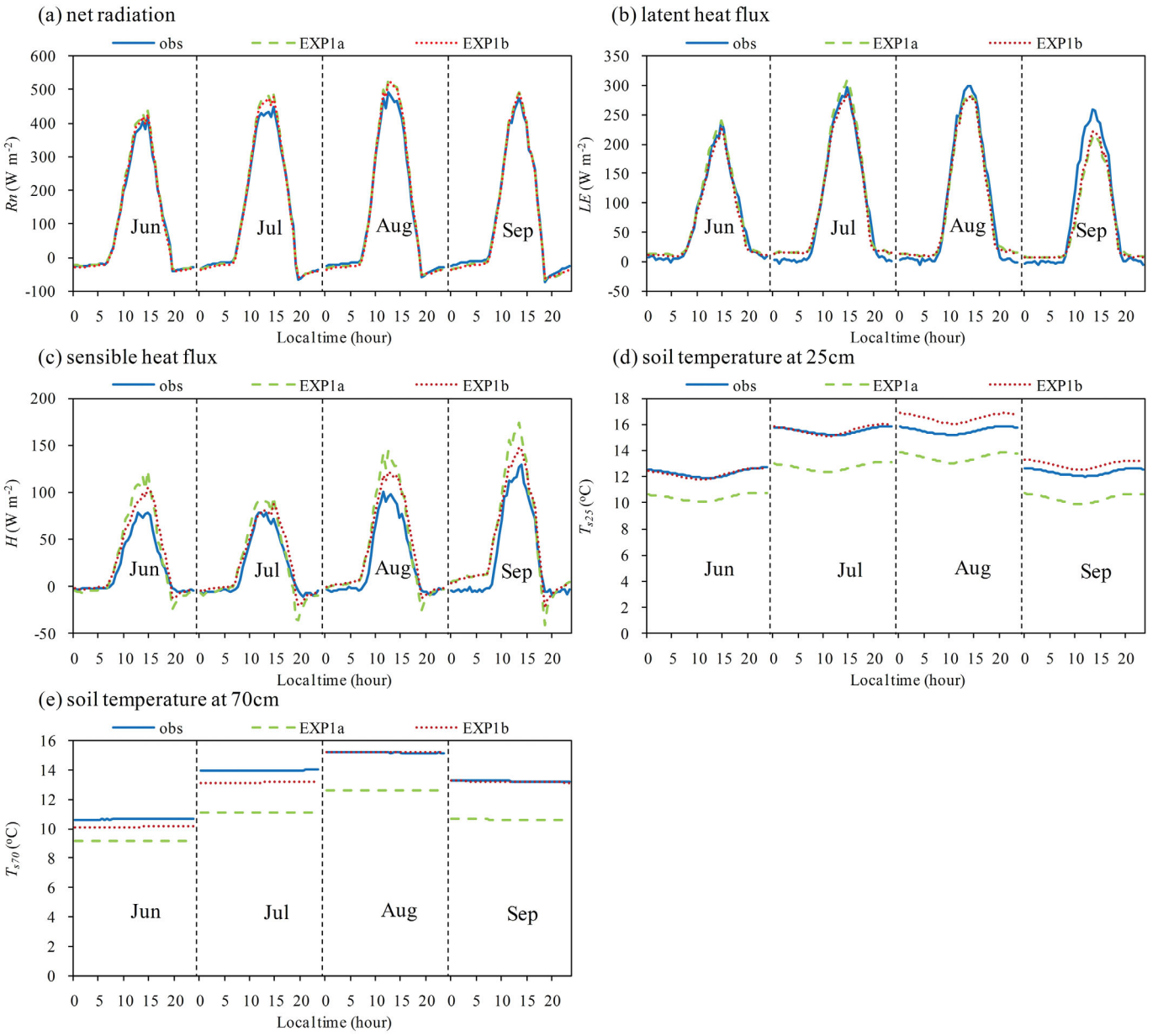

Figure 4. Monthly mean diurnal cycles for June, July, August and September of the measured and simulated (a) net incoming radiation, (b) latent heat flux, (c) sensible heat flux, (d) 25 cm, and (e) 70 cm soil temperature produced by Noah-MP using the default (EXP1a) and *Zeng et al.* [2005] (EXP1b) under-canopy turbulence transfer schemes.

more water from the upper layers. Hence, both EXP2b and EXP2c Noah-MP soil moisture simulations capture the dynamics measured at each soil depth in comparison to the default (EXP2a) much better.

Although modification of the root distribution function largely resolves the SM_5 overestimation during the dry-down, the SM_5 underestimation noted in the wet periods remains. In fact, Noah-MP with either the exponential or the asymptotic root distribution function produces somewhat larger underestimations as

Table 3. Root Mean Square Errors (RMSE) Computed Between the Measured and Simulated Net Incoming Radiation (R_n), Turbulent Heat Fluxes (LE and H), 25 cm and 70 cm Soil Temperature (T_{s25} and T_{s70}) Produced Using Noah-MP With the Two Under-Canopy Turbulence Transfer Schemes

RMSE	R_n (W m^{-2})	LE (W m^{-2})	H (W m^{-2})	T_{s25} (K)	T_{s70} (K)
EXP1a	17.23	27.96	25.72	2.32	2.51
EXP1b	16.67	25.43	18.69	0.81	0.48

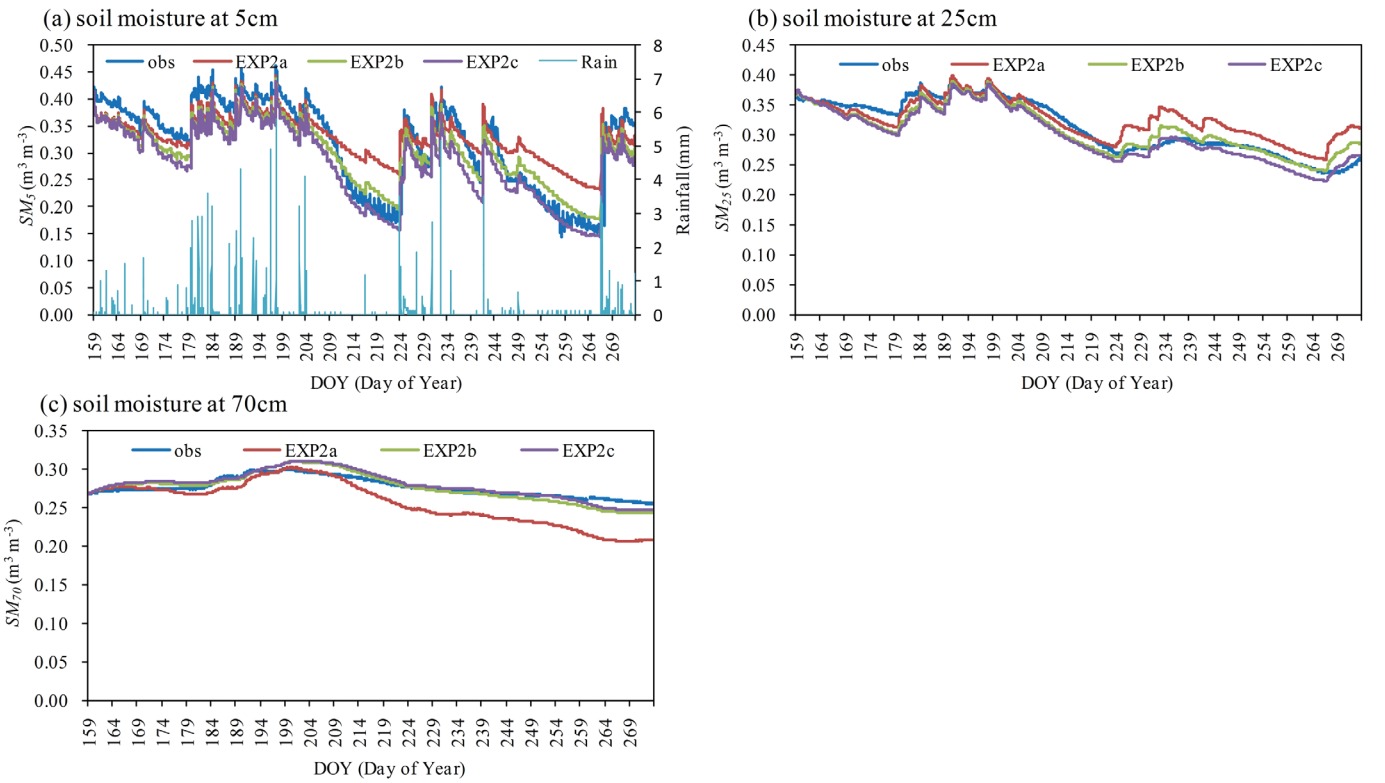

Figure 5. Time series of measurements and (a) 5 cm, (b) 25 cm, and (c) 70 cm soil moisture simulated with Noah-MP using three vertical root distribution functions from 8 June 2010 (DOY 159) to 30 September 2010 (DOY273).

compared to the default uniform function. As the soil moisture content under near-saturated conditions is largely constrained by the hydraulic properties, the relationship of the SM_5 underestimation with the soil hydraulic parameterization (e.g., porosity and hydraulic conductivity) is further discussed in section 6.2. In support of the analysis Table 4 lists the error statistics computed between the measured and simulated soil moisture profiles, i.e., the coefficient of determination (R^2), mean error (ME) and RMSE. The error statistics further confirm the amelioration of the soil moisture simulations following from distributing the majority of the roots in the upper layers (e.g., EXP2b and 2c) instead of uniformly across the soil profile. The most noticeable improvements are found for the deepest layer, e.g., SM_{70} with reductions in the absolute ME of about 100% and 85% and in the RMSE of about 70% and 74% with EXP2b and 2c, respectively. The exponential root distribution function is selected for the following experiments because it produces with default parameters (i.e., r_{ta} and r_{tb}) applied for global applications comparable results as the asymptotic function implemented with a specific parameter (i.e., β) for the Tibetan alpine meadow.

5.3. Soil Water Stress

Figure 6 shows time series of the measured and simulated SM_5 and SM_{70} by Noah-MP with six water stress (β_t) functions (EXP3a–3f, see Table 2) for which the exponential vertical root distribution function and under-canopy turbulence transfer scheme of *Zeng et al*. [2005] are used. Almost identical Noah-MP performances in simulating SM_5 are found with the six β_t functions during wet periods, for which the

Table 4. Error Statistics Computed Between the Measured and Simulated 5 cm, 25 cm, and 70 cm Soil Moisture (SM_5, SM_{25}, and SM_{70}) Produced by Noah-MP With Three Vertical Root Distribution Functions (EXP2a, 2b, and 2c)

	SM_5			SM_{25}			SM_{70}		
Experiments	R^2	ME (m^3 m^{-3})	RMSE (m^3 m^{-3})	R^2	ME (m^3 m^{-3})	RMSE (m^3 m^{-3})	R^2	ME (m^3 m^{-3})	RMSE (m^3 m^{-3})
EXP2a	0.851	0.010	0.050	0.769	0.012	0.025	0.801	−0.020	0.027
EXP2b	0.911	−0.016	0.037	0.882	−0.004	0.016	0.916	0.0	0.008
EXP2c	0.929	−0.036	0.044	0.933	−0.015	0.019	0.912	0.003	0.007

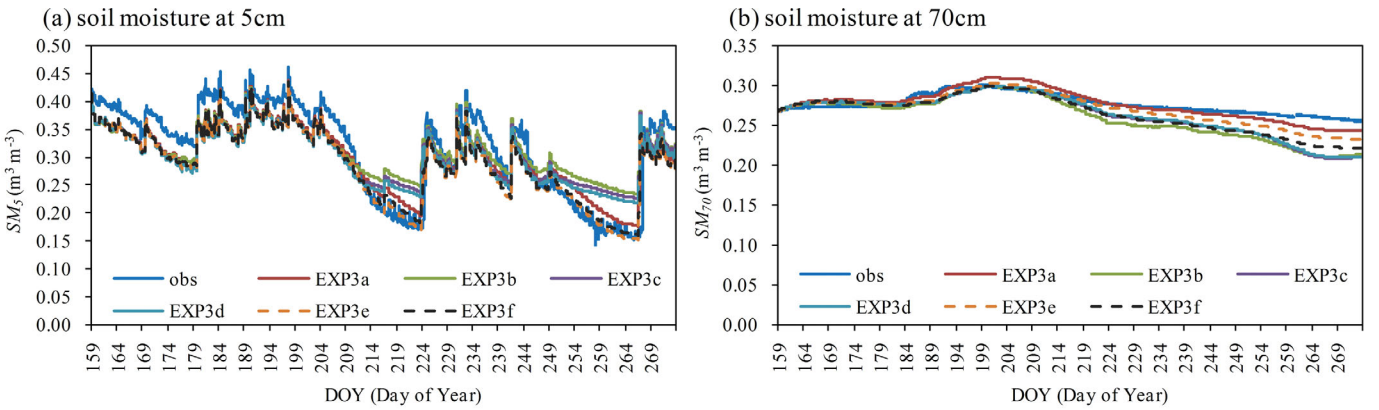

Figure 6. Time series of measured and (a) 5 cm and (b) 70 cm soil moisture simulated by Noah-MP with six water stress functions from 8 June 2010 (DOY 159) to 30 September 2010 (DOY273).

underestimation of the in situ measurements is characteristic as discussed above. Differences are, however, noted during the second and third dry-downs, i.e., DOYs 204–222 (23 July to 10 August) and DOYs 249–265 (6–22 September). The soil water potential (ψ)-based β_t functions (i.e., EXP3b, 3c, and 3d) consume less water for the transpiration from the surface layer than the soil moisture (θ)-based β_t functions (EXP3a, 3e and 3f) and, therefore, overestimates SM_5 during the two dry-downs. The explanation for this is that the ψ-based β_t functions enable the full opening of stomata toward the complete closure over a much smaller soil moisture range than the θ-based β_t functions (see Figure 3), which reduces the available water for transpiration. Since root water uptake from the top layer is shut shown under still fairly wet soil conditions with the ψ-based β_t functions, more water is extracted from the deep layers to fulfill the transpiration demands causing the underestimation noted for SM_{70} (Figure 6b). The nonlinear θ-based power function (EXP3e) and Jarvis's threshold approach (EXP3f) allow Noah-MP to extract more water and to capture better the SM_5 measurements during the two dry-downs as the cost of a somewhat larger SM_{70} underestimation.

Further Figure 7 presents time series of the measured and simulated *LE* by Noah-MP using two θ-based (EXP3a and 3e) and two ψ-based (EXP3b and 3d) β_t functions for an 8 day period of the third dry down, e.g., DOYs 255–262. Noah-MP underestimates *LE* with the linear θ-based β_t function (EXP3a) during the dry-downs, which explains the underestimation of the September mean diurnal *LE* cycle reported in section 5.1 (see Figure 4b). Implementation of any of the other β_t functions largely resolves this deficiency and provides an almost identically improved agreement with the *LE* measurements. The reason for this is that the linear θ-based β_t function produces a lower value of β_t and imposes, thus, a stronger constraint on plant transpiration as compared to the other functions (see Figure 3). The other β_t functions allow Noah-MP to transpire longer at a higher capacity and take up more water from the soil, which enable Noah-MP to produce *LE* simulations that better capture the measurements. Table 5 gives the error statistics (i.e., ME and RMSE) associated with EXP3a–3f computed between the measured and simulated soil moisture (SM_5 and SM_{70}) and turbulent heat fluxes (i.e., *LE* and *H*) for the two dry down episodes. The error statistics support that (i) the θ-based β_t functions (EXP3a, 3e, and 3f) perform better in simulating SM_5 with absolute ME and RMSE values twice as low as obtained with the ψ-based β_t functions (i.e., EXP3b, 3c, and 3d), and (ii) the linear θ-based β_t function (EXP3a) underestimates *LE* and overestimates *H*, which is resolved by implementing any of the other functions. Overall, both the nonlinear θ-based power function (EXP3e) and Jarvis's threshold approach (EXP3f) are best suited for providing reliable soil moisture and turbulent heat flux simulations simultaneously.

6. Sensitivity Test

6.1. Soil Water Stress Parameter

The above reported results in section 5.3 demonstrate that either of the two nonlinear θ-based β_t functions (e.g., power or Jarvis's) is the preferred choice for simultaneously simulating the turbulent heat fluxes and soil water flow reliably during dry-downs. Both options, however, adopt an *a priori* unknown empirical

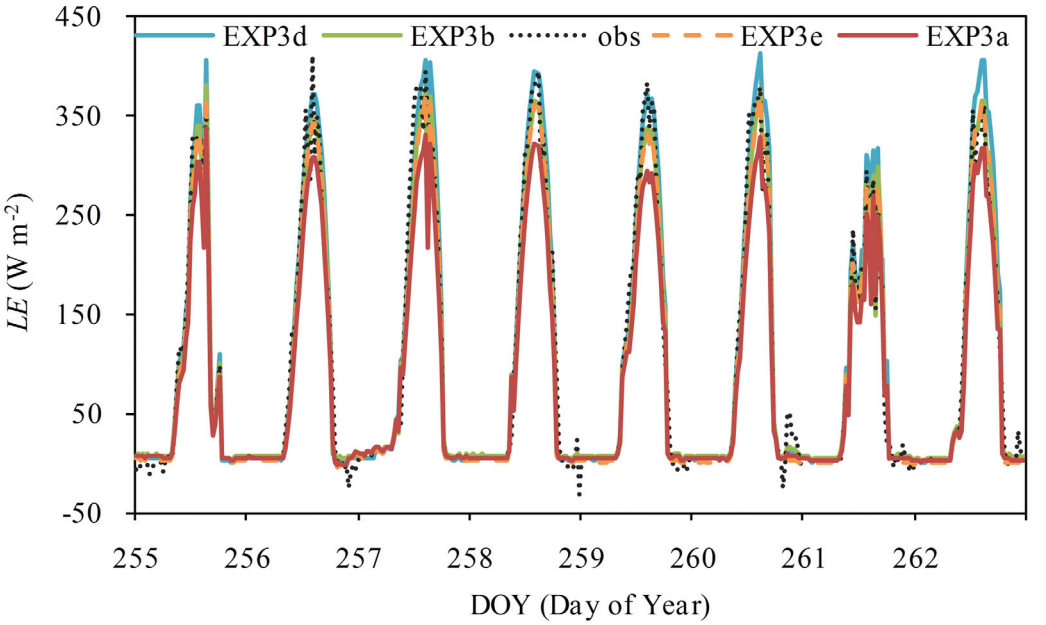

Figure 7. Time series of measured and latent heat flux simulated with Noah-MP using two moisture-based (EXP3a and 3e) and two potential-based (EXP3b and 3d) soil water stress functions for DOYs 255–262.

parameter, i.e., m for the power function (equation (19)) and threshold $\beta_{t,c}$ for Jarvis's approach (equation (20a)). Two series of experiments are performed to assess the sensitivity of the model results for the added parameters. For the first series of experiments Noah-MP is run with the power function using m equal to 1.0, 0.75, 0.50 and 0.25 (hereafter EXPS1a, EXPS1b, EXPS1c, and EXPS1d, respectively). Note that EXPS1a ($m = 1.0$) represents a linear β_t function as used in EXP3a, and EXPS1c ($m = 0.5$) is identical to EXP3e. The second series of experiments consists of Noah-MP model runs with Jarvis's approach using $\beta_{t,c}$ threshold values of 1.0, 0.75, 0.50 and 0.25 (hereafter EXPS2a, EXPS2b, EXPS2c, and EXPS2d, respectively), whereby EXPS2c ($\beta_{t,c} = 0.5$) is identical to EXP3f. Other model settings are as in EXP3a for both S1 and S2 experiment series.

Table 6 provides the error statistics computed between the measured and simulated turbulent heat fluxes (*LE* and *H*) and surface soil moisture (SM_5) of the S1 and S2 experiments for the two dry-downs (DOYs 204–222 and DOYs 249–265). Typically, lower m and $\beta_{t,c}$ values produce higher water stress factors (β_t's) and impose a weaker constraint on the root uptake (see Figure 3) allowing Noah-MP to transpire at a higher rate and extract more water from the soil. The ME's and RMSE's listed in Table 6 confirm that the selection of either m or $\beta_{t,c}$ equal to 0.5 (e.g., EXPS1c and S2c) is most suitable for a reliable reconstruction of the turbulent heat flux and soil moisture measurements, whereby Noah-MP with $m = 0.25$ generates similar yet slightly worse results. These findings demonstrate that the root uptake response to water stress is a nonlinear process, which is no surprise as plants also have the ability to take up water preferentially from the moist portions of the soil.

Table 5. Error Statistics Computed Between the Measured and Simulated 5 cm and 70 cm Soil Moisture (SM_5 and SM_{70}), as Well as Latent (*LE*) and Sensible (*H*) Heat Fluxes Produced by Noah-MP With Six Water Stress Functions (EXP3a–3f) for Two Dry-Down Periods, i.e., DOYs 204–222 and DOYs 249–265

	SM_5 ($m^3\ m^{-3}$)		SM_{70} ($m^3\ m^{-3}$)		*LE* (W m^{-2})		*H* (W m^{-2})	
Experiments	ME	RMSE	ME	RMSE	ME	RMSE	ME	RMSE
EXP3a	0.013	0.029	0.0	0.010	−13.58	30.13	12.22	19.71
EXP3b	0.039	0.058	−0.021	0.027	1.03	25.63	1.24	16.50
EXP3c	0.027	0.050	−0.017	0.025	6.89	26.98	−3.40	18.42
EXP3d	0.022	0.045	−0.017	0.024	7.47	27.31	−3.89	18.98
EXP3e	−0.008	0.022	−0.007	0.013	−3.47	26.05	4.21	16.78
EXP3f	−0.002	0.024	−0.017	0.021	1.47	26.07	0.49	16.76

Table 6. Error Statistics Computed Between the Measured and Simulated Turbulent Heat Fluxes (*LE* and *H*) and Surface Soil Moisture (SM_5) Produced by Noah-MP With the Power Stress Function Using *m* Equal to 1.0, 0.75, 0.50, and 0.25 (EXPS1a–1d, Respectively) and With Jarvis's Stress Function Using $\beta_{t,c}$ Equal to 1.0, 0.75, 0.50, and 0.25 (EXPS2a–2d, Respectively) for Two Dry-Down Periods (i.e., DOYs 204–222 and DOYs 249–265)

	LE (W m^{-2})		*H* (W m^{-2})		SM_5 (m^3 m^{-3})	
Experiments	ME	RMSE	ME	RMSE	ME	RMSE
EXPS1a	−13.58	30.13	12.22	19.71	0.013	0.029
EXPS1b	−8.51	27.44	8.19	17.69	0.004	0.024
EXPS1c	−3.47	26.05	4.21	16.78	−0.008	0.022
EXPS1d	1.24	26.18	0.46	17.21	−0.023	0.028
EXPS2a	−19.46	34.32	16.92	23.16	0.026	0.039
EXPS2b	−10.25	28.33	9.62	18.25	0.013	0.029
EXPS2c	1.47	26.07	0.49	16.76	−0.002	0.024
EXPS2d	8.08	28.11	−4.60	19.55	−0.007	0.023

6.2. Soil Hydraulic Parameter

Although substantial improvement is achieved in the Noah-MP performance in simulating soil states and fluxes (see section 5), the underestimation of surface soil moisture (SM_5) measured during the wet periods is not resolved by either of the selected schemes (see Figures 5a and 6a). In section 5.2, we argue that uncertainties in the selected soil hydraulic parameterization could form the explanation for the mismatch between the measurements and simulations. Notably, all previous experiments have been performed using mean values of the measured soil hydraulic parameters that does not account for existing variability present within the measurements especially for the surface layer (see Table 1). An additional numerical experiment is carried out to further investigate soil hydraulic parameter selection as cause for the underestimation of the measured SM_5. To achieve this aim experiments described in section 5.3 are repeated using the six soil water stress (β_t) functions, whereby Noah-MP is run using highest measured porosity (θ_s) and the lowest measured saturated hydraulic conductivity (K_s) of the surface layer to enlarge the water holding capacity (hereafter EXPS3a–S3f, respectively).

Figure 8 presents time series of the measured and simulated SM_5 produced by EXPS3a–S3f. Similar results are obtained as in section 5.3 where the ψ-based β_t functions (EXPS3b, S3c, and S3d) generally overestimate SM_5, while the nonlinear θ-based β_t functions (EXPS3e and S3f) better capture the SM_5 measurements during the dry-down periods. Further Noah-MP performance in simulating SM_5 during the wet periods is

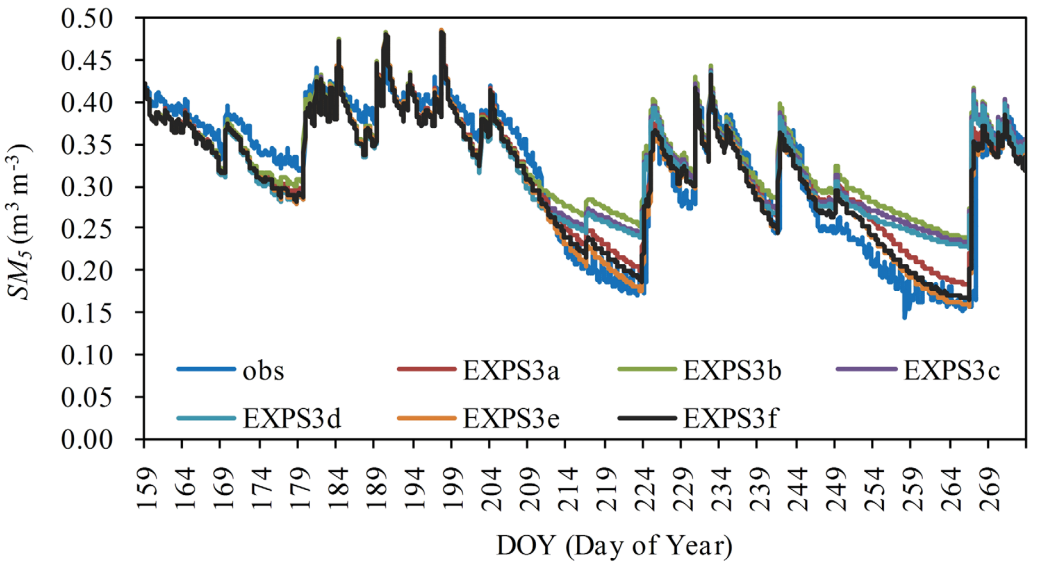

Figure 8. Time series of measured and simulated soil moisture at a 5 cm depth produced by EXPS3a–S3f with six water stress functions, and highest measured porosity and lowest measured saturated hydraulic conductivity of surface layer from 8 June 2010 (DOY 159) to 30 September 2010 (DOY273).

identical for the six β_t functions. More importantly, the SM_5 underestimation previously noted in Figure 6a (see section 5.3) is largely resolved by using the modified soil hydraulic parameters (i.e., θ_s and K_s). Hence, this also supports that rigor analyses of the uncertainties associated with the selected physics options as well as the adopted parameters is needed to achieve the optimum model performance as was recently emphasized in *Clark et al*. [2015b].

7. Conclusions

Noah-MP is a recently developed land surface model that adopts a framework for alternative parameterizations of specific physical processes, and provides a flexible way of adding new parameter choices and diagnosing their impact on model performance. In this paper, we expand Noah-MP with additional options for representing the under-canopy turbulence and root water uptake processes by including (i) an additional under-canopy turbulence scheme that interpolates the under-canopy turbulent transfer coefficients of thick canopy and bare soil [*Zeng et al*., 2005]; (ii) an exponential [*Zeng*, 2001] and an asymptotic [*Jackson et al*., 1996; *Y. Yang et al*., 2009] function defining the distribution of roots across the soil profile; and (iii) an updated soil water potential (ψ)-based [*Oleson et al*., 2013] function, a nonlinear soil moisture (θ)-based power function and a *Jarvis*'s [1989] threshold approach for determining the water stress (β_t), the latter allowing plants to transpire at full capacity in the presence of partial stress. The augmented Noah-MP is utilized to quantify the impact of the added under-canopy turbulence, vertical root distribution and soil water stress parameterizations on the model's ability in reproducing the measured turbulent heat fluxes and states (i.e., moisture and temperature) across the soil profile of an alpine meadow ecosystem in the northeastern part of the Tibetan Plateau.

The results show that Noah-MP with the original under-canopy turbulence scheme simulates the mean monthly diurnal net radiation and latent heat flux (*LE*) cycle reasonably well for the monsoon season (from June to September), but overestimates the sensible heat flux (*H*) and underestimates the soil temperature across the profile. These deficiencies are greatly resolved after replacing the default under-canopy turbulence scheme with the one proposed by *Zeng et al*. [2005] leading to RMSE reductions of about 27%, 65%, and 81% for *H*, and the 25 cm and 70 cm soil temperatures, respectively.

The exponential and asymptotic functions describing the vertical distribution of roots represent intuitively the characteristic abundance of roots near the soil surface of the Tibetan alpine meadows much better [*Y. Yang et al*., 2009]. As such, the Noah-MP runs with either of the two alternative root distribution functions are capable of extracting water volumes from the soil profile in a more realistic manner. With the default uniform root distribution, water uptake from the bottom layers is exaggerated causing an underestimation of the deep soil moisture and an overestimation of the soil moisture in the upper layers. Both exponential and asymptotic root distribution functions ensure that the appropriate amounts of water are extracted from the various soil layers leading to RMSE reductions up to more than 70% for the 70 cm soil moisture.

Additionally, the Noah-MP performance is assessed using in total six (three added) soil water stress functions of which three utilize soil moisture as state defining the stress level and the others employ the soil water potential. The comparison of the selected parameterizations demonstrates that the ψ-based functions, developed for models such as CLM [*Oleson et al*., 2004, 2013] and SSiB [*Xue et al*., 1991], impose a transition from root water uptake at full capacity toward a complete shut down over a rather small dynamic soil moisture range. This causes the overestimation of the soil moisture measured at a 5 cm depth and the underestimation of the deep soil moisture under dry down conditions. On the other hand, the constraint imposed on root water uptake via the linear θ-based function adopted originally by Noah [*Chen et al*., 1996] is too strong, especially in the early stages of water stress, leading to a *LE* underestimation and a complementary *H* overestimation. In this context, the newly added nonlinear θ-based power function and *Jarvis*'s [1989] threshold approach are found superior in providing simultaneously robust turbulent heat flux and soil moisture profile simulations. It should, however, be noted that the soil moisture measured at the 5 cm depth is generally underestimated during the wet periods by all the selected parameterizations.

Additional experiments have been performed to assess the sensitivity of the model results to the *a priori* unknown parameters introduced, i.e., *m* for the power function and $\beta_{t,c}$ for Jarvis's threshold approach. The results further support that the impact of water stress on root uptake is a nonlinear process following from

the fact that plants have the ability to take up water preferentially from the moist portions of the soil. Further, the impact of the uncertainty associated with the measured soil hydraulic parameters on the simulated soil moisture is assessed as well. This experiment demonstrates that the underestimation of soil moisture measured at depth of 5 cm during the wet periods can be largely revolved through increasing the water holding capacity of surface soil layer by modifying the hydraulic parameters, which highlights that appropriate physics options and parameter sets need to be selected to achieve the optimum model performance.

Overall, this study is exemplary for how amelioration of individual physical processes (e.g., under-canopy turbulence and root water uptake) can enhance the performance in simulating simultaneously energy and mass fluxes as well as soil states (e.g., temperature, moisture). An improved representation of physical processes as well as model parameters within land surface models is needed to enable reliable predictions of the impact of environmental changes, for instance driven by climate variability, on water, energy and nutrient cycles. The flexibility of selecting various physics options as provided by the multiparameterization framework of Noah-MP is imperative for accomplishing this task. Additional work is recommended to further study other dynamic root water uptake processes, such as hydraulic redistribution and water-tracking dynamic root growth apart from the preferential root water uptake investigated in this work.

Acknowledgments
This study was supported by funding from the FP7 CEOP-AEGIS and CORE-CLIMAX projects funded by the European Commission through the FP7 program, the Chinese Academy of Sciences Fellowship for Young International Scientists (grant 2012Y1ZA0013), the Key Research Program of the Chinese Academy of Sciences (grant KZZD-EW-13) and the National Natural Science Foundation of China (grant 41405079). The data sets used in this study were provided by Jun Wen in CAREERI/CAS. For data access, please contact the corresponding author (D. Zheng, d.zheng@utwente.nl).

References

Ajami, N. K., Q. Duan, and S. Sorooshian (2007), An integrated hydrologic Bayesian multimodel combination framework: Confronting input, parameter, and model structural uncertainty in hydrologic prediction, *Water Resour. Res.*, *43*, W01403, doi:10.1029/2005WR004745.

Brutsaert, W. H. (1982), *Evaporation Into the Atmosphere: Theory, History and Applications*, 316 pp., Springer, Boston.

Cai, X., Z.-L. Yang, C. H. David, G.-Y. Niu, and M. Rodell (2014), Hydrological evaluation of the Noah-MP land surface model for the Mississippi River Basin, *J. Geophys. Res. Atmos.*, *119*, 23–38, doi:10.1002/2013JD020792.

Campbell, G. S. (1974), A simple method for determining unsaturated conductivity from moisture retention data, *Soil Sci.*, *117*(6), 311–314.

Chen, F., K. Mitchell, J. Schaake, Y. Xue, H.-L. Pan, V. Koren, Q. Y. Duan, M. Ek, and A. Betts (1996), Modeling of land surface evaporation by four schemes and comparison with FIFE observations, *J. Geophys. Res.*, *101*(D3), 7251–7268.

Chen, X., Z. Su, Y. Ma, K. Yang, J. Wen, and Y. Zhang (2013), An Improvement of Roughness Height Parameterization of the Surface Energy Balance System (SEBS) over the Tibetan Plateau, *J. Appl. Meteorol. Climatol.*, *52*(3), 607–622.

Chen, Y., K. Yang, J. Qin, L. Zhao, W. Tang, and M. Han (2013), Evaluation of AMSR-E retrievals and GLDAS simulations against observations of a soil moisture network on the central Tibetan Plateau, *J. Geophys. Res. Atmos.*, *118*, 4466–4475, doi:10.1002/jgrd.50301.

Chen, Y., K. Yang, J. He, J. Qin, J. Shi, J. Du, and Q. He (2011), Improving land surface temperature modeling for dry land of China, *J. Geophys. Res.*, *116*, D20104, doi:10.1029/2011JD015921.

Clark, M. P., A. G. Slater, D. E. Rupp, R. A. Woods, J. A. Vrugt, H. V. Gupta, T. Wagener, and L. E. Hay (2008), Framework for Understanding Structural Errors (FUSE): A modular framework to diagnose differences between hydrological models, *Water Resour. Res.*, *44*, W00B02, doi:10.1029/2007WR006735.

Clark, M. P., et al. (2015a), A unified approach for process-based hydrologic modeling: 1. Modeling concept, *Water Resour. Res.*, *51*, 2498–2514, doi:10.1002/2015WR017198.

Clark, M. P., et al. (2015b), A unified approach for process-based hydrologic modeling: 2. Model implementation and case studies, *Water Resour. Res.*, *51*, 2515–2542, doi:10.1002/2015WR017200.

Clark, M. P., et al. (2015c), The structure for unifying multiple modeling alternatives (SUMMA), Version 1.0: Technical description, *NCAR Tech. Note NCAR/TN-514+STR*, National Center for Atmospheric Research, Boulder, Colo.

Dente, L., Z. Vekerdy, J. Wen, and Z. Su (2012), Maqu network for validation of satellite-derived soil moisture products, *Int. J. Appl. Earth Obs. Geoinf.*, *17*, 55–65.

de Rosnay, P., M. Bruen, and J. Polcher (2000), Sensitivity of surface fluxes to the number of layers in the soil model used in GCMs, *Geophys. Res. Lett.*, *27*(20), 3329–3332.

Dickinson, R. E., M. Shaikh, R. Bryant, and L. Graumlich (1998), Interactive canopies for a climate model, *J. Clim.*, *11*(11), 2823–2836.

Dirmeyer, P. A., X. Gao, M. Zhao, Z. Guo, T. Oki, and N. Hanasaki (2006), GSWP-2: Multimodel analysis and implications for our perception of the land surface, *Bull. Am. Meteorol. Soc.*, *87*(10), 1381–1397.

Ek, M. B., K. E. Mitchell, Y. Lin, E. Rogers, P. Grunmann, V. Koren, G. Gayno, and J. D. Tarpley (2003), Implementation of Noah land surface model advances in the National Centers for Environmental Prediction operational mesoscale Eta model, *J. Geophys. Res. Atmos.*, *108*(D22), 8851, doi:10.1029/2002JD003296.

Feddes, R. A., P. J. Kowalik, and H. Zaradny (1978), *Simulation of Field Water Use and Crop Yield*, John Wiley and Sons, N. Y.

Gale, M. R., and D. F. Grigal (1987), Vertical root distributions of northern tree species in relation to successional status, *Can. J. For. Res.*, *17*(8), 829–834.

Gayler, S., T. Wöhling, M. Grzeschik, J. Ingwersen, H.-D. Wizemann, K. Warrach-Sagi, P. Högy, S. Attinger, T. Streck, and V. Wulfmeyer (2014), Incorporating dynamic root growth enhances the performance of Noah-MP at two contrasting winter wheat field sites, *Water Resour. Res.*, *50*, 1337–1356, doi:10.1002/2013WR014634.

Immerzeel, W. W., L. P. H. van Beek, and M. F. P. Bierkens (2010), Climate change will affect the Asian Water Towers, *Science*, *328*(5984), 1382–1385.

Jackson, R. B., J. Canadell, J. R. Ehleringer, H. A. Mooney, O. E. Sala, and E. D. Schulze (1996), A global analysis of root distributions for terrestrial biomes, *Oecologia*, *108*(3), 389–411.

Jarvis, N. J. (1989), A simple empirical model of root water uptake, *J. Hydrol.*, *107*(1–4), 57–72.

Jiménez, C., et al. (2011), Global intercomparison of 12 land surface heat flux estimates, *J. Geophys. Res.*, *116*, D02102, doi:10.1029/2010JD014545.

Koike, T. (2004), The coordinated enhanced observing period––An initial step for integrated global water cycle observation, *WMO Bull.*, *53*(2), 115–121.

Koike, T., T. Yasunari, J. Wang, and T. Yao (1999), GAME-Tibet IOP summary report, in *Proceedings of the 1st International Workshop on GAME-Tibet*, Xi'an, China, 11–13 January 1999, pp. 1–2.
Koster, R. D., et al. (2004), Regions of strong coupling between soil moisture and precipitation, *Science*, *305*(5687), 1138–1140.
Kuhlmann, A., I. Neuweiler, S. E. A. T. M. van der Zee, and R. Helmig (2012), Influence of soil structure and root water uptake strategy on unsaturated flow in heterogeneous media, *Water Resour. Res.*, *48*, W02534, doi:10.1029/2011WR010651.
Lai, C.-T., and G. Katul (2000), The dynamic role of root-water uptake in coupling potential to actual transpiration, *Adv. Water Resour.*, *23*(4), 427–439.
Lawrence, P. J., and T. N. Chase (2009), Climate Impacts of Making Evapotranspiration in the Community Land Model (CLM3) Consistent with the Simple Biosphere Model (SiB), *J. Hydrometeorol.*, *10*(2), 374–394.
Li, H., M. Huang, M. S. Wigmosta, Y. Ke, A. M. Coleman, L. R. Leung, A. Wang, and D. M. Ricciuto (2011), Evaluating runoff simulations from the Community Land Model 4.0 using observations from flux towers and a mountainous watershed, *J. Geophys. Res.*, *116*, D24120, doi:10.1029/2011JD016276.
Li, K. Y., R. De Jong, and J. B. Boisvert (2001), An exponential root-water-uptake model with water stress compensation, *J. Hydrol.*, *252*(1–4), 189–204.
Li, K. Y., R. De Jong, M. T. Coe, and N. Ramankutty (2006), Root-water-uptake based upon a new water stress reduction and an asymptotic root distribution function, *Earth Interact.*, *10*(14), 1–22.
Li, L., Y.-P. Wang, Q. Yu, B. Pak, D. Eamus, J. Yan, E. van Gorsel, and I. T. Baker (2012), Improving the responses of the Australian community land surface model (CABLE) to seasonal drought, *J. Geophys. Res.*, *117*, G04002, doi:10.1029/2012JG002038.
Li, L., C. van der Tol, X. Chen, C. Jing, B. Su, G. Luo, and X. Tian (2013), Representing the root water uptake process in the Common Land Model for better simulating the energy and water vapour fluxes in a Central Asian desert ecosystem, *J. Hydrol.*, *502*, 145–155.
Luo, X., X. Liang, and H. R. McCarthy (2013), VIC+ for water-limited conditions: A study of biological and hydrological processes and their interactions in soil-plant-atmosphere continuum, *Water Resour. Res.*, *49*, 7711–7732, doi:10.1002/2012WR012851.
Ma, Y., S. Kang, L. Zhu, B. Xu, L. Tian, and T. Yao (2008), ROOF OF THE WORLD: Tibetan Observation and Research Platform, *Bull. Am. Meteorol. Soc.*, *89*(10), 1487–1492.
Ma, Y., et al. (2009), Recent advances on the study of atmosphere-land interaction observations on the Tibetan Plateau, *Hydrol. Earth Syst. Sci.*, *13*(7), 1103–1111.
Mahat, V., D. G. Tarboton, and N. P. Molotch (2013), Testing above- and below-canopy representations of turbulent fluxes in an energy balance snowmelt model, *Water Resour. Res.*, *49*, 1107–1122, doi:10.1002/wrcr.20073.
Mahrt, L., and H. Pan (1984), A two-layer model of soil hydrology, *Boundary Layer Meteorol.*, *29*(1), 1–20.
Maxwell, R. M., and N. L. Miller (2005), Development of a coupled land surface and groundwater model, *J. Hydrometeorol.*, *6*(3), 233–247.
Niu, G.-Y., and Z.-L. Yang (2004), Effects of vegetation canopy processes on snow surface energy and mass balances, *J. Geophys. Res.*, *109*, D23111, doi:10.1029/2004JD004884.
Niu, G.-Y., Z.-L. Yang, R. E. Dickinson, and L. E. Gulden (2005), A simple TOPMODEL-based runoff parameterization (SIMTOP) for use in global climate models, *J. Geophys. Res.*, *110*, D21106, doi:10.1029/2005JD006111.
Niu, G.-Y., Z.-L. Yang, R. E. Dickinson, L. E. Gulden, and H. Su (2007), Development of a simple groundwater model for use in climate models and evaluation with Gravity Recovery and Climate Experiment data, *J. Geophys. Res.*, *112*, D07103, doi:10.1029/2006JD007522.
Niu, G.-Y., et al. (2011), The community Noah land surface model with multiparameterization options (Noah-MP): 1. Model description and evaluation with local-scale measurements, *J. Geophys. Res.*, *116*, D12109, doi:10.1029/2010JD015139.
Niu, G.-Y., C. Paniconi, P. A. Troch, R. L. Scott, M. Durcik, X. Zeng, T. Huxman, and D. C. Goodrich (2014), An integrated modelling framework of catchment-scale ecohydrological processes: 1. Model description and tests over an energy-limited watershed, *Ecohydrology*, *7*(2), 427–439.
Oleson, K., Y. Dai, G. B. Bonan, M. Bosilovichm, R. Dickinson, P. Dirmeyer, F. Hoffman, P. Houser, S. Levis, and G. Y. Niu (2004), Technical description of the Community Land Model (CLM), *NCAR Tech. Note NCAR/TN-461+STR*, National Center for Atmospheric Research, Boulder, Colo.
Oleson, K., et al. (2013), Technical description of version 4.5 of the Community Land Model (CLM), *NCAR Tech. Note NCAR/TN-503+STR*, National Center for Atmospheric Research, Boulder, Colo.
Pan, H. L., and L. Mahrt (1987), Interaction between soil hydrology and boundary-layer development, *Boundary Layer Meteorol.*, *38*(1–2), 185–202.
Piao, S., K. Tan, H. Nan, P. Ciais, J. Fang, T. Wang, N. Vuichard, and B. Zhu (2012), Impacts of climate and CO2 changes on the vegetation growth and carbon balance of Qinghai–Tibetan grasslands over the past five decades, *Global Planet. Change*, *98–99*, 73–80.
Pitman, A. J., Y. Xia, M. Leplastrier, and A. Henderson-Sellers (2003), The CHAmeleon Surface Model: Description and use with the PILPS phase 2(e) forcing data, *Global Planet. Change*, *38*(1–2), 121–135.
Rodriguez-Iturbe, I., P. D'Odorico, A. Porporato, and L. Ridolfi (1999), On the spatial and temporal links between vegetation, climate, and soil moisture, *Water Resour. Res.*, *35*(12), 3709–3722.
Sakaguchi, K., and X. Zeng (2009), Effects of soil wetness, plant litter, and under-canopy atmospheric stability on ground evaporation in the Community Land Model (CLM3.5), *J. Geophys. Res.*, *114*, D01107, doi:10.1029/2008JD010834.
Schaake, J. C., V. I. Koren, Q.-Y. Duan, K. Mitchell, and F. Chen (1996), Simple water balance model for estimating runoff at different spatial and temporal scales, *J. Geophys. Res.*, *101*(D3), 7461–7475.
Schymanski, S. J., M. Sivapalan, M. L. Roderick, L. B. Hutley, and J. Beringer (2009), An optimality-based model of the dynamic feedbacks between natural vegetation and the water balance, *Water Resour. Res.*, *45*, W01412, doi:10.1029/2008WR006841.
Scott, R. L., W. L. Cable, and K. R. Hultine (2008), The ecohydrologic significance of hydraulic redistribution in a semiarid savanna, *Water Resour. Res.*, *44*, W02440, doi:10.1029/2007WR006149.
Sellers, P. J., Y. Mintz, Y. C. Sud, and A. Dalcher (1986), A Simple Biosphere Model (SIB) for use within general circulation models, *J. Atmos. Sci.*, *43*(6), 505–531.
Seneviratne, S. I., D. Luthi, M. Litschi, and C. Schar (2006), Land-atmosphere coupling and climate change in Europe, *Nature*, *443*(7108), 205–209.
Sivandran, G., and R. L. Bras (2013), Dynamic root distributions in ecohydrological modeling: A case study at Walnut Gulch Experimental Watershed, *Water Resour. Res.*, *49*, 3292–3305, doi:10.1002/wrcr.20245.
Su, Z., J. Wen, L. Dente, R. van der Velde, L. Wang, Y. Ma, K. Yang, and Z. Hu (2011), The Tibetan Plateau observatory of plateau scale soil moisture and soil temperature (Tibet-Obs) for quantifying uncertainties in coarse resolution satellite and model products, *Hydrol. Earth Syst. Sci.*, *15*(7), 2303–2316.
Su, Z., P. de Rosnay, J. Wen, L. Wang, and Y. Zeng (2013), Evaluation of ECMWF's soil moisture analyses using observations on the Tibetan Plateau, *J. Geophys. Res. Atmos.*, *118*, 5304–5318, doi:10.1002/jgrd.50468.

van der Tol, C., A. G. C. A. Meesters, A. J. Dolman, and M. J. Waterloo (2008), Optimum vegetation characteristics, assimilation, and transpiration during a dry season: 1. Model description, *Water Resour. Res.*, *44*, W03421, doi:10.1029/2007WR006241.
van der Velde, R., Z. Su, M. Ek, M. Rodell, and Y. Ma (2009), Influence of thermodynamic soil and vegetation parameterizations on the simulation of soil temperature states and surface fluxes by the Noah LSM over a Tibetan plateau site, *Hydrol. Earth Syst. Sci.*, *13*(6), 759–777.
Verhoef, A., and G. Egea (2014), Modeling plant transpiration under limited soil water: Comparison of different plant and soil hydraulic parameterizations and preliminary implications for their use in land surface models, *Agric. For. Meteorol.*, *191*, 22–32.
Vrugt, J. A., M. T. van Wijk, J. W. Hopmans, and J. Šimunek (2001), One-, two-, and three-dimensional root water uptake functions for transient modeling, *Water Resour. Res.*, *37*(10), 2457–2470.
Xia, Y., J. Sheffield, M. B. Ek, J. Dong, N. Chaney, H. Wei, J. Meng, and E. F. Wood (2014), Evaluation of multi-model simulated soil moisture in NLDAS-2, *J. Hydrol.*, *512*, 107–125.
Xue, B.-L., et al. (2013), Modeling the land surface water and energy cycles of a mesoscale watershed in the central Tibetan Plateau during summer with a distributed hydrological model, *J. Geophys. Res. Atmos.*, *118*, 8857–8868, doi:10.1002/jgrd.50696.
Xue, Y., P. J. Sellers, J. L. Kinter, and J. Shukla (1991), A Simplified Biosphere Model for global climate studies, *J. Clim.*, *4*(3), 345–364.
Yang, K., T. Koike, B. Ye, and L. Bastidas (2005), Inverse analysis of the role of soil vertical heterogeneity in controlling surface soil state and energy partition, *J. Geophys. Res.*, *110*, D08101, doi:10.1029/2004JD005500.
Yang, K., Y. Y. Chen, and J. Qin (2009), Some practical notes on the land surface modeling in the Tibetan Plateau, *Hydrol. Earth Syst. Sci.*, *13*(5), 687–701.
Yang, K., et al. (2013), A multiscale soil moisture and freeze–thaw monitoring network on the third pole, *Bull. Am. Meteorol. Soc.*, *94*(12), 1907–1916.
Yang, K., H. Wu, J. Qin, C. Lin, W. Tang, and Y. Chen (2014), Recent climate changes over the Tibetan Plateau and their impacts on energy and water cycle: A review, *Global Planet. Change*, *112*, 79–91.
Yang, Y., J. Fang, C. Ji, and W. Han (2009), Above- and belowground biomass allocation in Tibetan grasslands, *J. Veg. Sci.*, *20*(1), 177–184.
Yang, Z.-L., and G.-Y. Niu (2003), The versatile integrator of surface and atmosphere processes: Part 1. Model description, *Global Planet. Change*, *38*(1–2), 175–189.
Yang, Z.-L., et al. (2011), The community Noah land surface model with multiparameterization options (Noah-MP): 2. Evaluation over global river basins, *J. Geophys. Res. 116*, D12110, doi:10.1029/2010JD015140.
Zeng, X. (2001), Global vegetation root distribution for land modeling, *J. Hydrometeorol.*, *2*(5), 525–530.
Zeng, X., M. Shaikh, Y. Dai, R. E. Dickinson and R. Myneni (2002), Coupling of the Common Land Model to the NCAR Community Climate Model, *J. Clim.*, *15*(14), 1832–1854.
Zeng, X., M. Barlage, R. E. Dickinson, Y. Dai, G. Wang and K. Oleson (2005), Treatment of undercanopy turbulence in land models, *J. Clim.*, *18*(23), 5086–5094.
Zeng, X., Z. Wang and A. Wang (2012), Surface skin temperature and the interplay between sensible and ground heat fluxes over arid regions, *J. Hydrometeorol.*, *13*(4), 1359–1370.
Zeng, Y., Z. Su, L. Wan and J. Wen (2011), A simulation analysis of the advective effect on evaporation using a two-phase heat and mass flow model, *Water Resour. Res.*, *47*, W10529, doi:10.1029/2011WR010701.
Zheng, D., R. van der Velde, Z. Su, M. J. Booij, A. Y. Hoekstra, and J. Wen (2014), Assessment of roughness length schemes implemented within the Noah Land Surface Model for high-altitude regions, *J. Hydrometeorol.*, *15*(3), 921–937.
Zheng, Z., and G. Wang (2007), Modeling the dynamic root water uptake and its hydrological impact at the Reserva Jaru site in Amazonia, *J. Geophys. Res.*, *112*, G04012, doi:10.1029/2007JG000413.
Zhou, X., P. Zhao, J. Chen, L. Chen, and W. Li (2009), Impacts of thermodynamic processes over the Tibetan Plateau on the Northern Hemispheric climate, *Sci. China Ser. D Earth Sci.*, *52*(11), 1679–1693.